NORTHWESTERN UNIVERSITY

Neural Mechanisms of Olfactory Categorization and Navigation in the Human Brain

A DISSERTATION

SUBMITTED TO THE GRADUATE SCHOOL

IN PARTIAL FULFILLMENT OF THE REQUIREENTS

for the degree

DOCTOR OF PHILOSOPHY

Field of Neuroscience

By

Xiaojun Bao

EVANSTON, ILLINOIS

June 2018

Abstract

Neural Mechanisms of Olfactory Categorization and Navigation in the Human Brain

Xiaojun Bao (包笑君)

The brains of humans and animals have the amazing capability of extracting abstract relationships between external stimuli efficiently. Knowing such regularities helps us compute and react to novel information flexibly without prior experience. The olfactory system is no exception. Animals need to infer commonalities across different odors sharing similar meaning, while preserving individual distinctions across these odors. They must also locate and predict sources of odors to optimize their proximity to the odor-emitting objects. The neural mechanisms underlying these critical olfactory cognitions are still full of questions. In two independent fMRI experiments, we investigated how the human brain represents 1) categorically organized odor objects, and 2) two-dimensional odor space constructed by two-odorant mixtures.

In the first experiment, we took advantage of the anatomical organization of the olfactory system and delivered the GABA(B) receptor agonist baclofen to suppress associative input to human piriform cortex. Multi-voxel pattern analyses revealed that baclofen disrupted pattern separation of within-category odors in the piriform cortex, and disrupted pattern separation of odor categories in the orbitofrontal cortex (OFC) and the hippocampus.

In the second experiment, we uncovered evidence of grid-like coding with a two-dimensional virtual landscape constructed only of odors. We found that humans can learn to navigate through

an odor space, and that the internal maps of the space take the form of periodic, hexagonally symmetric patterns in the entorhinal cortex, the ventromedial prefrontal cortex, and the anterior piriform cortex, consistent with a grid-like arrangement.

Results from these experiments should advance our understanding of coding mechanisms by which the olfactory brain represents odors with relational organizations in different applications. They complement and extend earlier literature on olfactory cognition, and advance olfaction as a model system for further studies of relational memory.

Acknowledgments

This work would not have been possible without guidance and support from all the incredible people throughout my graduate school journey. First and foremost, I would like to thank my advisor, Dr. Jay Gottfried. It has been a privilege to receive your mentorship and scientific training. Thank you for fulfilling my childhood dream of working with a giant mind-reading machine, and for having your door always open whenever I got lost.

I would like to thank my committee members, Drs. Thorsten Kahnt, Marsel Mesulam, Jelena Radulovic, and Paul Reber, for their invaluable feedback and advice. Special thanks to Thorsten, for being an immensely helpful collaborator who made significant contributions to my research projects. I'm grateful for the training and funding support I received from Dr. John Disterhoft and others via the Mechanism of Aging and Dementia Training Program.

Thank you to past and present members of the Gottfried Lab: Nicholas Bowman, Pei-Ching Chang, Sydni Cole, Eva Gjorgieva, Katherina Hauner, James Howard, Isabel Hutchison, Heidi Jiang, Katherine Khatibi, Olga Lacki, Shayna Levine, Daria Porter, Lisa Qu, Louise Raguet, Laura Shanahan, Joanna Wu, and Christina Zelano. Additional thanks to Louise, Sydni, Eva, and Laura for help in data collection, and thanks to James for teaching me fMRI analysis A to Z.

Thank you to my NUIN pals: Xiaowen Yu, Meriel Owen, and Eileen McIver. It would have been a lonely journey without your company. Thanks to my NU friends: Sali Liu, for our tennis mornings, Yeqing Yang, for our guitar nights, Yiwen Zhu, for your hot-pot, Xiaobao Li, for your ribs, Fangke Xu, for your gorgeous deserts, Junjing Deng, for your tea. Because of you, I never

had a hungry stomach or soul.

To my parents, thank you for your unconditional love and support. You are the reason for my existence.

Finally, I thank Nick, for his love, and for correcting my English.

Table of Contents

Abstract 3

Acknowledgments 5

Lists of Tables and Figures 9

Chapter 1: General introduction and background 10

1.1 The olfactory system: an overview 10

1.2 On olfactory categorization: the effect of GABA(B) receptor activation on the balance of discrimination and generalization 14

1.3 On olfactory navigation: grid-like representation of a mental map 20

1.4 Specific aims 24

Chapter 2: The role of piriform associative connections in odor categorization 26

2.1 Abstract 26

2.2 Introduction 26

2.3 Methods 30

2.4 Results 37

2.5 Discussion 50

Chapter 3: Grid-like neural representations support olfactory navigation of a two-dimensional Euclidean space 57

3.1 Abstract 57

3.2 Introduction 58

3.3 Methods 64

3.4 Results 75

3.5 Discussion 82

Chapter 4: Conclusions and future directions 84

References 89

Lists of Tables and Figures

Table 2.1 Behavioral performance..... 40

Figure 1.1 Circuit diagram of the piriform cortex. 15

Figure 1.2 Basic parameters of grid fields. 23

Figure 2.1 Experimental design. 38

Figure 2.2 Effect of baclofen on subjective sleepiness. 39

Figure 2.3 Subjects successfully classified odors into their relevant categories. 42

Figure 2.4 Ensemble pattern coding of odor category information at baseline (pre-baclofen session). 44

Figure 2.5 Baclofen effect on odor pattern changes in PPC. 46

Figure 2.6 Baclofen effect on odor pattern changes in OFC and pHIP. 48

Figure 2.7 Visual control experiment. 49

Figure 3.1 Experimental design and navigation performance. 60

Figure 3.2 Odor trajectory θ distributions across mixtures. 62

Figure 3.3 Illustration of different trial types. 63

Figure 3.4 Grid axis angle φ estimated from vmPFC ROI for each subject. 72

Figure 3.5 Multi-voxel pattern analysis (MVPA) method pipeline. 74

Figure 3.6 Grid-like signals during odor navigation. 78

Figure 3.7 Dissociation between odor trajectory and visual trajectory. 79

Figure 3.8 Grid-like ensemble activity in entorhinal cortex. 81

Chapter 1: General introduction and background

1.1 The olfactory system: an overview

Here is the recipe of the smell of Spring Festival (normally between late January and February) in my hometown Jiaxing, a third-tier city in Southeast China: the odor of gunpowder from finished firecrackers, the odor of deep-fried pork meatballs cooked with soy sauce, and the odor of maltose from street vendors, mixed in dry air at a temperature around 5°C. How this unmistakable smell sensation emerges from networks of neurons, and how it eventually defines a time and space in my mind, is a fascinating mystery.

Olfaction is a chemical sense that detects air-borne odorant molecules in the environment and forms the sense of smell. The transduction of odor information starts with odorous molecules activating olfactory sensory neurons (OSNs) in our nose as we breath or sniff, which creates airflow and brings those molecules to the olfactory epithelium lying on the roof of our nasal cavity. At the epithelium, odorant molecules bind to olfactory receptors at the sensory endings (many hair-like cilia) of OSNs. Olfactory receptors are members of G protein-coupled receptors (GPCRs). Each OSN expresses only one receptor subtype out of 400 possible receptors in humans (about 1,000 in rodents) (Malnic et al 2004, Zhang & Firestein 2002). A single odorant can bind to multiple receptor subtypes with varying affinities, and a single receptor can bind to different odorants. Moreover, the binding mechanism between molecules and receptors is elusive. The most widely accepted theory is that a molecule's smell character depends on its molecular structure, molecular size, functional groups, etc. Alternatively, the (rather controversial) vibration theory proposes that odor molecular recognition lies in the vibrational frequency tuning curves of olfactory receptors in the infrared range (Franco et al 2011).

Therefore, unlike color vision and tone perception where the stimulus-percept problem is well understood, it has been extremely difficult to predict odor percept from the molecular descriptors of odor stimuli (Keller et al 2017).

Once activated, OSNs send action potentials along their axons, which form the olfactory nerve (the first cranial nerve), and synapse near the surface of the olfactory bulb. In the epithelium, OSN subtypes are segregated into a small number of broad yet circumscribed expression zones, with stochastic distribution within a given zone (Ressler et al 1993, Vassar et al 1993). In contrast, the same OSN subtype terminates on just one or a few glomeruli within the bulb (Ressler et al 1994, Vassar et al 1994). A glomerulus is a spherical structure where synapses form between the axons of OSNs and the dendrites of mitral and tufted cells (projection cells) and periglomerular cells (inhibitory interneurons). The convergence of information from OSNs makes the individual glomerulus a molecular feature-detecting unit, and has the likely advantage of enhancing sensitivity by summation of low level signals (Mori et al 1999). The olfactory bulb also contains several other inhibitory interneurons, the largest population being granule cells, which receive top-down cortical feedback and modulate mitral/tufted cells. The interneurons are important for establishing lateral inhibitory circuits, gain control, and top-down regulations (Imai 2014).

Axonal projections from mitral/tufted cells in the olfactory bulb travel through the lateral olfactory tract and arrive at several cortical and subcortical areas, collectively called primary olfactory cortex, including: the anterior olfactory nucleus, olfactory tubercle, piriform cortex, amygdala, and rostral entorhinal cortex (Gottfried 2010). Different from other sensory systems,

the olfactory pathway does not require a thalamic relay before reaching cortical areas. Among the regions that receive direct input from the olfactory bulb, the piriform cortex is the largest target, and is usually split into anterior and posterior subdivisions based on their anatomical and functional distinctions. Anatomically, the anterior piriform cortex (APC) receives more abundant afferent projections from the olfactory bulb whereas the posterior piriform cortex (PPC) receives more associative fiber inputs arising elsewhere (Haberly 2001). Functionally, the APC generally represents odor identity and the PPC encodes information about perceptual quality (Gottfried et al 2006, Howard et al 2009). In contrast to the convergent organization in the olfactory bulb, axons from individual glomeruli project diffusely to the piriform cortex without obvious spatial bias (Ghosh et al 2011, Miyamichi et al 2011, Sosulski et al 2011). The distributive projection pattern offers an anatomic substrate for combinatorial integration of information from the bulb. Functional mapping of odor-evoked activity in rodents (Cattarelli et al 1988, Illig & Haberly 2003, Rennaker et al 2007, Stettler & Axel 2009) and humans (Howard et al 2009) confirmed that different monomolecular odorants elicit unique and distributed ensemble patterns of neural activity in the piriform cortex.

Downstream of the primary olfactory cortex is an extended network of brain areas, including the orbitofrontal cortex (OFC), agranular insula, hypothalamus, amygdala, perirhinal cortex, the hippocampal formation, striatum, thalamus, etc. (Carmichael et al 1994, Courtiol & Wilson 2014, Illig 2005, Johnson et al 2000, Majak et al 2004, Shipley & Ennis 1996) Most of these connections are bidirectional, like those between the olfactory bulb and primary olfactory cortex. It takes as few as three synapses for the chemical information to reach the limbic and prefrontal areas, which support emotion, learning and memory, expectation and attention. The close link

between odor input and high-order associative systems implies that odor percepts are more reliant on (and modified by) experience and emotional or cognitive states compared to other sensory modalities.

The olfactory system is also unique among sensory systems in sending information predominantly to the ipsilateral hemisphere. Studies investigating the olfactory sense in unilateral neglect patients have provided insights into the nature of sensory attention and awareness. Unilateral neglect is a disorder resulting most commonly from brain damage of the right hemisphere, particularly of the right parietal lobe. The right parietal lobe appears to be able to direct attention to both left and right sides of space, while the left hemisphere seems to be responsible mostly for guiding attention toward contralateral (right) space (Mesulam 1981). Split-brain patients and patients with strokes and brain injuries to the right cerebral hemisphere often fail to respond to stimuli presented to the left side of the body and space. Two major theories have been raised to explain the mechanism: the sensory theory states that unilateral neglect involves attenuated afferent input to the right hemisphere from the contralateral side of the body and space; in contrast, the representational theory argues that it is due to a diminished internal representation, which is not dependent on sensory input. Since the olfactory pathways to the cerebral hemispheres are not crossed before reaching the primary olfactory cortex, it provides a unique mechanism to test the two theories. If the neglect is caused by a sensory loss, it should occur on the ipsilateral side, whereas an internal representation deficit should cause a contralateral neglect. A clinical case by Mesulam (Mesulam 1981) described a patient with right parietal brain damage who exhibited left-sided extinction of olfactory stimuli, which was later

supported by a group study (Bellas et al 1988). These results provided strong evidence for the representational theory.

1.2 On olfactory categorization: the effect of GABA(B) receptor activation on the balance of discrimination and generalization

One important function of olfactory cognition is categorization: to recognize odors as members of categories, which reflect the conceptual relationships among odors. The abilities to discriminate between prey and predator, food and nonfood, ingroups and outsiders, are essential functions for survival. At the same time, no two sniffs are the same. Even from the same source, the odorant concentration and volatility, as well as airflow (sniff) patterns, can change with time. Therefore, being able to generalize odors according to similar perceptual quality or context helps to optimize behavioral decisions more efficiently.

Previous research has suggested that the piriform cortex contains neural correlates of odor quality and category perceptions. Howard et al. found that odors with different perceptual qualities evoked different fMRI activity in the form of spatially distributed (multi-voxel) patterns in human piriform cortex. Moreover, perceived quality similarities lined up with piriform pattern similarities, and both resulted in the same categorical organization (Howard et al 2009). Importantly, odor quality perceptions are experience dependent and cannot always be read out solely from olfactory bulb's glomeruli response profiles. Rats had to go through extensive training to learn to discriminate highly overlapping odor mixtures which were initially indistinguishable, or to ignore the normally detectable differences between mixtures. Single unit recordings from the piriform cortex showed learning-induced pattern separation (discrimination)

and pattern completion (generalization), depending on the task demands, whereas such bidirectional plasticity was absent in the olfactory bulb (Chapuis & Wilson 2012). The same effect was also found in human subjects. With an aversive conditioning paradigm, subjects were able to discriminate two mirror-image molecules that initially smelled the same. In parallel, fMRI activity patterns in piriform cortex became more distinct after learning (Li et al 2008).

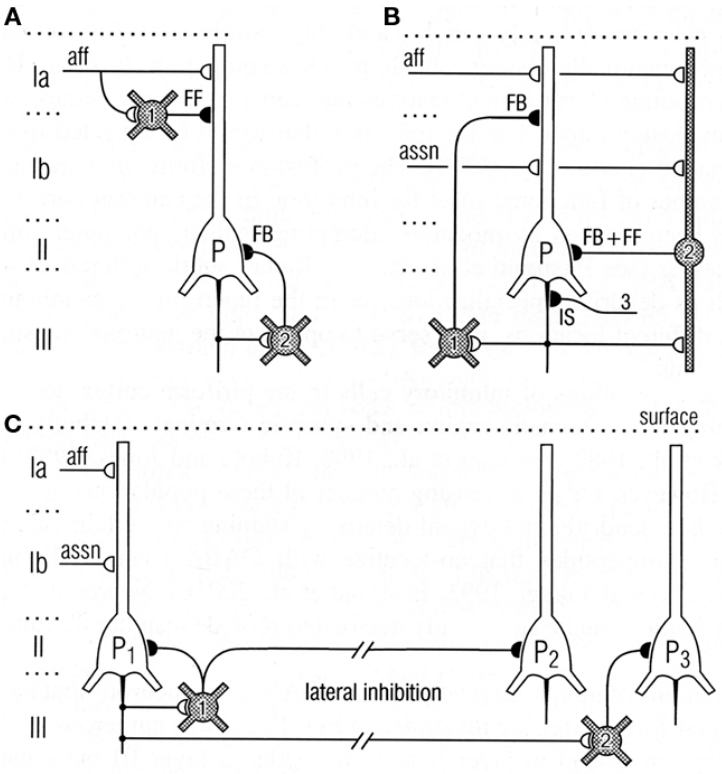

Figure 1.1 Circuit diagram of the piriform cortex.
(A) Feedforward (FF) inhibitory (I) circuit from lateral olfactory tract afferents (aff) and feedback (FB) inhibitory circuit onto pyramidal cells (P). **(B)** Feedback and feedforward circuits from pyramidal cell axons, including inhibitory control of the initial segment (IS); assn, association fibers. **(C)** Pathways for lateral inhibition, through long axons of basket cell onto distant pyramidal cell, or long axon collateral of pyramidal cell onto distant basket cell. Open profiles: excitatory synaptic action; filled profiles: inhibitory synaptic action. (Shepherd 2011)

The structure of the piriform cortex is strikingly similar to that of the hippocampus. Both take the form of a phylogenetically conserved three-layered allocortex (Vaughan & Jackson 2014), and

share comparable laminar and microcircuit organizations. The most superficial layer (layer I) of piriform cortex is a plexiform layer consisting of two sublayers: layer Ia receives axons from the olfactory bulb (*afferent input*), and layer Ib consists of associative axons from other neurons in piriform cortex as well as from other olfactory cortical regions (*associative input*). Layers II and III are cellular layers that house principal cells. Multiple classes of GABAergic inhibitory interneurons are found across all layers in the piriform cortex. They provide various feed-forward and feedback inhibition onto the pyramidal cells (Franks et al 2011, Stokes & Isaacson 2010, Suzuki & Bekkers 2012) (**Fig. 1.1**).

In addition to the laminar segregation of afferent and associative inputs in layer I, there is also laminar selectivity of synaptic suppression by the GABA(B) receptor agonist baclofen in both piriform cortex and hippocampus. GABA(B) receptors are metabotropic receptors that mediate slow and prolonged synaptic inhibition through a G-protein associated second messenger system. They were demonstrated on presynaptic terminals (where they serve as autoreceptors) to influence transmitter release by suppressing Ca^{2+} conductance. They are also located postsynaptically, where their activation produces an increase in membrane K^{+} conductance and associated slow hyperpolarization (Bowery 1993, Bowery et al 2002). In both the piriform cortex and the hippocampus, functional GABA(B) receptors are absent on afferent fiber terminals. Applications of baclofen, a highly selective agonist for GABA(B) receptors, strongly depresses associative transmission with no effect on afferent-evoked responses (Lanthorn & Cotman 1981, Tang & Hasselmo 1994). Therefore, baclofen has been used as a pharmacological tool in rodent studies to examine the role of associative connections in odor coding in the piriform cortex, by selectively blocking associative inputs and sparing afferent inputs (Barnes & Wilson 2014,

Gerrard et al 2018, Poo & Isaacson 2011). For the first experiment in this dissertation, we used baclofen in humans to inspect the role of associative inputs in category coding in the piriform cortex via the same mechanism.

Odor category codes have been reported in higher-order brain areas downstream of the piriform cortex in human fMRI studies. In an olfactory deprivation study, Wu et al. found category codes in multivoxel ensemble patterns in the OFC at baseline, which became decorrelated after 7-days of nostril occlusion, and returned to baseline after recovery (Wu et al 2012). Using a paired-associates learning paradigm, subjects perceptually reorganized novel ambiguous odors into categories, and category specific patterns emerged in the piriform, OFC, insular, and perirhinal cortices (Qu et al 2016). With this evidence, it is reasonable to expect that higher-order association areas would contain odor category codes, which could be changed by baclofen as the result of either the direct action of the drug on-site, or the downstream effect from piriform changes.

Baclofen, commonly administered orally, was originally approved by the FDA in 1977 as a muscle relaxant and antispastic (Brennan et al 2013). Its off-label use has been investigated for treatment of alcohol and drug addiction (Dupouy et al 2014, Franklin et al 2012, Franklin et al 2011, Kahn et al 2009, Terrier et al 2011, Young et al 2014). For a 50-mg dose of oral tablet, the expected drug concentration in the cerebrospinal fluid is 106 ng/ml (0.5 μM) after 0.5-1.5 h (Terrier et al 2011). Because baclofen would be delivered orally and have a systemic effect, and because GABA(B) receptors are distributed throughout the brain (Bowery et al 1987, Chu et al 1990), the drug could possibly influence all stages the olfactory brain responsible for odor

categorization function.

GABA(B) expression in the olfactory bulb. The first synapse of the olfactory pathway – where olfactory nerve axons terminate in olfactory bulb glomeruli – is modulated by GABA(B) receptors presynaptically. This effect is strong for intraglomerular feedback inhibition via periglomerular interneurons, but weak for interglomerular lateral inhibition mediated by juxtaglomerular interneurons (McGann et al 2005). Baclofen action at this level is more likely to have effects on input sensitivity rather than spatial maps of glomerular input. In the deeper layers of the bulb, there are local dendrodendritic circuits formed between lateral dendrites of mitral cells and the dendrites of granule cells, potentially mediating lateral inhibition between mitral cells. Mitral cells release glutamate onto the dendritic spines of granule cells, which in turn release GABA back onto mitral dendrites. This reciprocal inhibition is modulated by GABA(B) autoreceptors on granule cells (Isaacson & Vitten 2003). Furthermore, postsynaptic effects of baclofen on mitral cells are minor (Aroniadou-Anderjaska et al 2000). It is difficult to analyze all potential action sites and deduce the net effect of baclofen on the olfactory bulb responses, but evidence so far suggests that GABA(B) receptors in the bulb serve as a gain control and modulate signal-to-noise ratio and input sensitivity (Palouzier-Paulignan et al 2002). Unfortunately, the human olfactory bulb has been a black box to fMRI, due to its size and high susceptibility to artifacts resulting from the adjacent air sinus.

GABA(B) expression in piriform cortex. Activation of presynaptic GABA(B) receptors on the terminals of associative fibers reduces associative inputs onto piriform pyramidal cells. Presynaptic GABA(B) receptors are also expressed on the axons of GABAergic interneurons,

whose activation produces disinhibition of principal cells. Meanwhile, activation of postsynaptic GABA(B) receptors hyperpolarizes principal cells and reduces their intrinsic excitability. Again, the gross effect of baclofen on the piriform circuit would be hard to compute from all the elements. However, except for the presynaptic effect on input fibers, the other potential effects have no selectivity in the event of afferent input vs. associative input. Therefore, baclofen can still create imbalance between afferent and associative input strengths, and can be used to test the effect of weakened associative connection on odor coding. Without odor stimuli, superfusion of baclofen reduced spontaneous firing initially, but promoted synchronous epileptiform activity later, a seemingly dichotomous modulation of circuit excitability. It is suggested that this biphasic effect was possibly due to the variable modulator roles of GABA(B) receptors as the agonist diffused deeper into the piriform cortex (Gerrard et al 2018). While looking at odor-evoked activation of piriform pyramidal cells, application of baclofen narrowed the tuning properties of their responses (becoming more odor selective) (Poo & Isaacson 2011). However, these results were observed in anesthetized animals, and could be very different from the awake state. In a fear conditioning paradigm in rats, baclofen infusion into the piriform cortex after learning led to enhanced generalization of odor-evoked freezing behavior (Barnes & Wilson 2014), potentially due to an impairment in odor discrimination.

GABA(B) expression in hippocampus. As in the piriform cortex, baclofen selectively suppresses synaptic transmission at synapses arising from CA3 pyramidal cells (intrinsic fibers) more than transmission at performant path synapses (afferent inputs). Computational modeling shows that GABA(B) receptor modulation is associated with the endogenous 4-10 Hz theta rhythm, a prominent field oscillation in the hippocampal system during exploratory behavior and learning

(Wallenstein et al 1998). Additionally, it is suggested to play a role in both pattern completion and pattern separation depending on the task demand (Sohal & Hasselmo 1998, Wallenstein & Hasselmo 1997). Therefore, baclofen could act on hippocampus directly and influence its function in learning and memory tasks in which discontinuous items must be associated.

The first experiment in this dissertation examines the effect of GABA(B) receptor activation (by baclofen) on odor categorization in the human brain. Because of the caveat mentioned above, the results observed are interpreted with caution. We focused on multiple odor category coding regions, including the piriform cortex. The effect in each region could be the result of changes in the local circuit, secondary effects from different sources, or connectivity and state changes on a larger inter-regional network scale.

1.3 On olfactory navigation: grid-like representation of a mental map

Knowing the "what" of odors lays the foundation for a second function: knowing the "where" of odors. Spatial orientation to odor sources (or away from them) is the next essential function for survival after discriminating prey from predator, food from nonfood, ingroups from outsiders. Honeybee recruits locate food sources by olfaction, as odor of the source accumulates in the hive (Wenner et al 1969). Homing pigeons rely on odor distributions in the atmosphere to navigate home (Gagliardo 2013, Wallraff 2000). As humans, because of our advanced visual system, we do not tend to think about olfaction when we think about spatial navigation. However, humans can follow a scent trail like a dog, or point to the source of a distant odor from the center of an open field. The performance of both tasks benefited from inter-nostril comparisons (Porter et al 2007). Humans can also define a location in space as a coordinate on an odor space (Jacobs et al

2015). The second experiment in this dissertation aims to examine the neural mechanism of how an odor space is encoded in the human brain.

It is necessary to define the concept of “odor space” used in this work. Due to the large number of combinations between the molecular variability and olfactory receptor types, a considerable amount of research has been dedicated to determine the dimensionality of the “odor space”, which is a hyperdimensional space made up by hundreds of descriptors about the perceived odor quality (Bushdid et al 2014, Castro et al 2013, Keller et al 2017, Koulakov et al 2011, Meister 2015, Schiffman 1974, Snitz et al 2013). Here, we use “odor space” to refer to a mental map of the spatial relationships among odor distributions in the physical world.

A simplest model of an odor space can be an orthogonal coordinate space created by plumes from two odorants (A and B), which increase in concentration in two perpendicular directions (axes). Lucia Jacobs proposed two possible spatial logics for such an odor space (Jacobs 2012). First, in a natural environment, odor concentration decreases with distance from the source, and our percept of an odor is intensity-dependent. The intensity gradient of two odorants can form local neighborhoods of different mixture combinations, e.g. low A + low B, low A + high B, high A + high B, etc. Second, certain odor mixtures can be perceived as synthetic objects, making landmarks in the space and increasing the spatial resolution. It was shown that humans can infer location from such an Euclidean odor space (Jacobs et al 2015). For the second experiment in this dissertation, we want to explore how the odor space is mapped in the brain.

Research on spatial navigation has identified the medial temporal lobe – the hippocampal system and the adjacent perirhinal, entorhinal, and parahippocampal corteces – to be essential for spatial memory, with milestone discoveries of place cells in the hippocampus (O'Keefe & Dostrovsky 1971) and grid cells in the entorhinal cortex (Hafting et al 2005). A place cell responds to a random place field in the environment without a topographic pattern. On the other hand, a grid cell responds to a periodic triangular array tiling the environment. The firing structure of grid cells can be described by three parameters: grid scale (the distance between grid fields), grid orientation (the rotation of grid axes), and grid phase (the x-y locations of firing vertices) (**Fig. 1.2**). Grid cells in the same animal have random spatial phase, but modular grid orientation. This means there are dominant population of grid cells in the entorhinal cortex sharing a common grid-axis orientation (Stensola et al 2012). In addition, there are conjunctive grid × head-direction cells in the deeper layers, which fire more while the animal is moving along the grid-axis (Doeller et al 2010, Sargolini et al 2006). These particular features allow the group activities of grid cells to be detected by macroscopic fMRI signals (Doeller et al 2010). Briefly, when subjects move in a direction aligned with the grid orientation, they will hit firing vertices of the grid cells more frequently than a direction aligned at 30° to the grid (misaligned with the grid orientation). Theoretically, the resulting fMRI signal will show dynamic response as the function of moving direction: a cosine waveform with 60° periodicity, which can be detected by in-phase and quadrature decomposition (for details about analysis techniques, see Chapter 3.3 Methods).

Following the introduction of the analysis technique in 2010, grid-like representations of spaces of varying nature were reported in multiple human fMRI studies. For example, these were detected when subjects navigated a virtual space (Doeller et al 2010, Kunz et al 2015) or

imagined navigating such a space (Bellmund et al 2016, Horner et al 2016). They coded the visual field when subjects were making gaze movement in a visual space (Julian et al 2018, Nau et al 2018), which was supported by single cell recordings in primates (Killian et al 2012). They were also found in abstract space navigation, when an arbitrary "bird map" was constructed by stretching and shrinking the neck length and the leg length of a bird (Constantinescu et al 2016). These results are supporting evidence of the concept of the cognitive map, which was introduced by Edward Tolman as an internalized neural representation of physical or metaphorical locations (Tolman 1948). Therefore, we expected that a grid-like code might also be employed in mapping a space defined by odors.

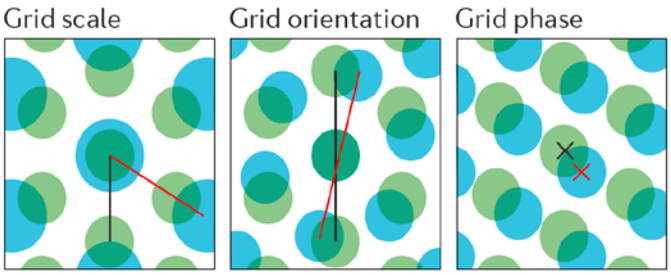

Figure 1.2 Basic parameters of grid fields.
Cartoons of firing patterns of pairs of grid cells (shown in blue and green), illustrating the parameters of grid scale, grid orientation and grid phase. Lines in left and middle panels indicate two axes of the grid pattern (which define grid orientation); crosses in the panel on the right indicate grid phase (*x*–*y* location of grid fields). (Moser et al 2014)

So far, the few rodent studies testing for hexagonal profiles outside of ERC have only identified grid cells in the presubiculum and parasubiculum (Boccara et al 2010). However, single-neuron recordings from humans have reported grid-like spiking patterns in the cingulate cortex (Jacobs et al 2013), and fMRI studies have identified grid-like signals in the medial prefrontal, posterior parietal and lateral temporal cortices (Constantinescu et al 2016, Doeller et al 2010). When

testing grid-like fMRI signals during odor space navigation, we focused on the entorhinal cortex, but also reasoned that such signals might appear in other brain areas as well.

It is worth noting that the olfactory portion of entorhinal cortex receives direct afferent input from the olfactory bulb, confined to the lateral subdivision in rodents (Haberly & Price 1977), which exhibits little spatial selectivity (Hargreaves et al 2005), whereas grid cells are found exclusively in the medial entorhinal cortex. Along the longitudinal axis, the olfactory projection covers the whole extent of the entorhinal cortex in rodents. However, it decreases substantially in macaques, comprising roughly 15% of the entorhinal cortex in the rostromedial subfield. The human homologue defined by topological and cytoarchitectonic criteria may be even smaller (Insausti et al 2002).

The major entorhinal subdivisions – lateral and medial in rodents, corresponding to the anterior-posterior axis in humans – have differential connectivity with the perirhinal cortex vs. the parahippocampal cortex, and in turn with the anterior-posterior hippocampus (Maass et al 2015, Navarro Schroder et al 2015). Therefore, it is posited that the entorhinal cortex is the hub where two memory networks meet: an anterior-temporal system sensitive to object information converges on perirhinal cortex, and a posterior-medial system sensitive to spatial information converges on the parahippocampal cortex (Ranganath & Ritchey 2012). Thus, the entorhinal cortex could be the site where “content” binds to “context”.

1.4 Specific aims

In the following two chapters I describe two experiments attempting to tackle the neural

mechanisms of two critical functions of the olfactory system: categorization and navigation. Seemingly two distinct functions, they fall under the same overarching problem of how the brain represents odor stimuli with either discrete relational structure (different identities within categories) or continuous relational structure (different intensities/identities in space).

In the first experiment, I used a simple odor categorization paradigm and administered the GABA(B) receptor agonist, baclofen, in a double-blind, placebo-controlled group design, to examine the drug effect on odor-evoked fMRI activity patterns in human olfactory brain areas. Because baclofen selectively inhibits associative connections while sparing afferent input in the piriform cortex, I aimed to gain insights on the role of piriform associative connections in cortical coding of odor category.

In the second experiment, I constructed an arbitrary Euclidean odor space using two odorants with varying intensities, as a model of odor intensity gradients encountered in the natural environment. I applied a task analogous to common spatial navigation task in human fMRI experiments, and tested whether we could detect grid-like neural activities in the brain representing the odor space.

Chapter 2: The role of piriform associative connections in odor categorization

2.1 Abstract

Distributed neural activity patterns are widely proposed to underlie object identification and categorization in the brain. In the olfactory domain, pattern-based representations of odor objects are encoded in piriform cortex. This region receives both afferent and associative inputs, though their relative contributions to odor perception are poorly understood. Here, we combined a placebo-controlled pharmacological fMRI paradigm with multivariate pattern analyses to test the role of associative connections in sustaining olfactory categorical representations. Administration of baclofen, a GABA(B) agonist known to attenuate piriform associative inputs, interfered with within-category pattern separation in piriform cortex, and the magnitude of this drug-induced change predicted perceptual alterations in fine-odor discrimination performance. Comparatively, baclofen reduced pattern separation between odor categories in orbitofrontal cortex, and impeded within-category generalization in hippocampus. Our findings suggest that odor categorization is a dynamic process concurrently engaging stimulus discrimination and generalization at different stages of olfactory information processing, and highlight the importance of associative networks in maintaining categorical boundaries.

2.2 Introduction

Object categorization is an adaptive function of the brain, allowing organisms to sort information from the external world into behaviorally relevant classes. Importantly, sensory systems must generalize across different objects sharing similar features, but at the same time maintain the specificity of individual objects and categories (Riesenhuber & Poggio 2000, Roach 1978). Mechanisms of pattern recognition have been proposed to underlie the neural basis of object

categorization, which requires a balance between generalizing inputs across a certain range of variations (known as *pattern completion*) and discriminating between distinct inputs (known as *pattern separation*) (Chapuis & Wilson 2012, Haberly 2001, Riesenhuber & Poggio 2000, Wilson & Sullivan 2011). Such computations can be achieved by associating sensory inputs with internal templates that are established through a lifetime of experience and encoded into memory (Bar 2007).

Most neuroscientific research on pattern recognition has concentrated on the visual system, where associative areas in the visual ventral stream and the CA3 region of the hippocampus have been shown to support processes of object categorization (Haxby et al 2001, Riesenhuber & Poggio 2000, Yassa & Stark 2011). In the olfactory system, information in a whiff of scented air is transformed into distributed patterns of neural activity in the piriform cortex, with both animal and human studies demonstrating that different odor objects evoke distinguishable ensemble activity patterns without spatial topography (Bekkers & Suzuki 2013, Gottfried 2010, Howard et al 2009, Stettler & Axel 2009, Wilson & Sullivan 2011). Recent work has revealed that fMRI multivariate patterns in posterior piriform cortex (PPC) encode not only odor identity, but also category information (e.g., minty or woody), whereby odor patterns belonging to the same category are more similar (more overlapping) than those across different categories (Howard et al 2009). Despite these insights, the mechanisms by which olfactory inputs are organized into categorical percepts through their associations with olfactory cortical areas are poorly understood.

The neural architecture of the piriform cortex makes it an attractive model for investigating

mechanisms of odor object recognition. As the largest subregion of primary olfactory cortex, the piriform cortex receives afferent (bottom-up) inputs from the olfactory bulb through the lateral olfactory tract, and extensive associative (top-down) inputs from higher-order association areas such as orbitofrontal cortex (OFC), amygdala, and entorhinal cortex (Carmichael et al 1994, Haberly & Price 1978, Insausti et al 1987, Insausti et al 2002, Johnson et al 2000). This convergence of bottom-up and top-down projections, along with the presence of dense recurrent collaterals, is thought to support olfactory pattern recognition and associative learning (Haberly 2001, Haberly & Bower 1989, Wilson 2009). For example, when confronted with highly overlapping odor mixtures, rats can learn to discriminate or ignore detectable differences between these mixtures, with piriform activity patterns exhibiting either separation (enhanced discrimination) or completion (enhanced generalization), respectively (Chapuis & Wilson 2012). Evidence from humans has also pointed to PPC as a substrate for odor discrimination (Li et al 2008) and categorization (Howard et al 2009). Together these findings suggest that piriform cortex is capable of modulating pattern representations along a discrimination-generalization spectrum in order to encode behaviorally adaptive meaning through perceptual experience.

While theoretical modelling and empirical evidence propose that piriform associative connections are essential for odor recognition (Haberly 2001), few studies have explicitly investigated the relative contributions of afferent inputs versus associative networks in supporting odor categorization. In a previous fMRI study, human subjects were deprived of afferent sensory input for one week, resulting in a reduction of odor-evoked mean activity in PPC, without alteration of pattern-based piriform representations of odor categories (Wu et al 2012). Here we address the inverse question, namely, how attenuation of piriform associative

connections influences odor category coding in primary sensory regions and higher-order cortical areas.

To this end, we took advantage of the GABA(B) receptor agonist, baclofen, to modify the relative balance between afferent and associative inputs within piriform cortex. Baclofen selectively suppresses synaptic transmission of association fibers into piriform cortex, but leaves afferent inputs from the olfactory bulb unaffected (Tang & Hasselmo 1994). In vivo local application of baclofen in the piriform cortex of anesthetized rats modified the strength of odor-evoked responses of pyramidal neurons, by blocking broadly-tuned neurons and increasing odor-selective responses (Poo & Isaacson 2011). In behaving animals, injection of baclofen into the piriform cortex following an olfactory fear conditioning session resulted in fear memory generalization, indicating that piriform associative connections are essential for consolidation of stimulus-specific memories (Barnes & Wilson 2014).

Inspired by these animal studies, we conducted a double-blind, placebo-controlled drug study in human subjects to examine fMRI ensemble representations of familiar odor categories before and after treatment with baclofen. Given that odor object codes take the form of distributed ensemble patterns, we used multivariate fMRI analyses to characterize baclofen effects in olfactory areas found to represent categorical information. The placebo group served as a control to account for session-effect confounds between pre- and post-drug phases of the study. As such, we examined the effects of baclofen by comparing pre-to-post changes relative to those observed in placebo subjects (i.e., group-by-session interaction). We predicted that baclofen would disrupt associative connections, leading to perceptual and neural reorganization of odor categories in

piriform cortex and in olfactory downstream areas including OFC, amygdala, entorhinal cortex, and hippocampus.

2.3 Methods

Subjects

We obtained informed consent from 36 subjects (mean age, 25 years; 18 baclofen and 18 placebo, with equal numbers of men and women in each group) to participate in this study, which was approved by the Northwestern University Institutional Review Board. Subjects were right-handed nonsmokers with no history of significant medical illness, psychiatric disorder, or olfactory dysfunction. Four female baclofen subjects were excluded from the results due to either excessive movement or falling asleep in the scanner, leaving a total of 14 baclofen subjects.

Study design

The total length of the experiment spanned 5 consecutive days. Following enrollment, subjects were randomly assigned to the baclofen (n = 14) or placebo (n = 18) group by the research pharmacy at Northwestern Memorial Hospital. Experimenters and subjects were both blinded to these assignments. Subjects took 10mg of baclofen or placebo on the first day and progressively increased the dosage by 10mg per day to reach 50mg at day 5. On day 1 before drug administration, subjects underwent pre-drug baseline tests including cognition, olfactory psychophysics, and fMRI imaging measures. On day 5 after medication, subjects completed post-drug tests which were the same as the pre-drug session.

Odor stimuli and delivery

Six odorants were used in the fMRI odor categorization experiment and included two "citrus" smells (R-(+)-limonene and Citral), two "mint" smells (L-Menthol and Methyl Salicylate), and two "wood" smells (Cedrol and Vetiver Acetate). For the fine odor discrimination task outside the scanner, two perceptually similar isomers, α- and β-pinene (5% diluted in mineral oil), were used in an olfactory three-way forced choice triangular task. Odors were delivered using a custom-built olfactometer. In this system, clean air or odorized air was directed towards subjects (wearing a nasal mask) via Teflon tubing at a rate of 3L/min.

General cognitive measures

On days 1 and 5, subjects were tested on four cognitive measures before olfactory testing and fMRI scanning: (1) Mini-mental state examination (MMSE), a short questionnaire used to measure cognition impairment (Folstein et al 1975); (2) an auditory digit span test (in forward and backward order) to assess short-term memory; (3) Trail Making Test B as a measure of visual attention and cognitive flexibility(Bowie & Harvey 2006); and (4) subjective report of degree of alertness using the Stanford Sleepiness Scale (SSS) (Hoddes et al 1973), which ranges from "Feeling active, vital, alert, or wide awake" (1 point) to "No longer fighting sleep, sleep onset soon; having dream-like thoughts" (7 points).

Olfactory psychophysical measures

Four behavioral measures were tested outside of the scanner. (1) Odor detection thresholds and (2) odor identification ability were assessed using Sniffin' Sticks (Burghart) and the University of Pennsylvania Smell Identification Test (UPSIT, Sensonics), respectively (Doty et al 1984,

Hummel et al 1997). (3) A triangular odor discrimination task was performed to assess the ability to discriminate α- and β-pinene (Li et al 2008). (4) For the six odorants used in the fMRI odor categorization experiment, visual analog ratings of odor intensity (anchors, “undetectable” and “extremely intense”), pleasantness (anchors, “dislike”, ”neutral”, and “like”), pair-wise similarity of odor quality (anchors, “not alike at all” and “identical”) (Howard et al 2009) were collected. Subjects also rated the applicability of descriptors of the three categories (citrus, mint and wood) with anchors (“not at all” and “extremely citrusy/minty/woody”).

fMRI olfactory and visual categorization tasks

Subjects underwent an odor categorization task designed to assess the multivoxel pattern specificity of odor-evoked fMRI activity across pre- and post-drug sessions. The task was divided into six 8-min runs of 28 trials each, during which the six odors were presented for 4 or 5 trials (depending on the run). On each trial, subjects were presented a visual sniff cue prompting them to sniff. Odor stimuli were presented for 1.5s, with a 13-s stimulus-onset asynchrony (SOA). Each odor was presented 28 times in pseudorandom order. Four out of the 28 trials in each run were randomly chosen as “catch trials”, where subjects were asked to indicate the category of the received odor with a mouse click. The catch trials were not included in the fMRI pattern analysis. The total task lasted for 48min.

Subjects also performed a visual categorization task which was parallel to the olfactory version with the equivalent number of trials and runs, and visual and olfactory runs were interleaved. On each trial, an image (from a total of six possible images, **Fig. 2.7a**) was presented for 0.5s, with a jittered interval of 3-4 s between trials. The visual fMRI data were absent from 1 male placebo

subject due to technical problems during the experiment.

fMRI visual ROI localizer scan

A separate functional localizer scan was performed to identify regions of image-evoked activity to be used in the visual pattern analysis. This scan was done in the pre-drug session, in which subjects were shown seven 20-s blocks of images (0.3s presentation and 0.7s inter-stimulus interval) with 20-s resting gaps between blocks. Each block contained one of six object categories (chairs, houses, teapots, cars, keys, and scissors) or scrambled version of the same images. The scrambled images were created by dividing the images into 20 × 20 unit grids and shuffling the units. During the image presentation blocks, subjects performed a one-back detection task by pressing a button to maintain their focus and attention.

Respiratory monitoring and analysis

Breathing behavior was monitored during olfactory scanning with a spirometer (affixed to the nasal mask) measuring the flow of air during inhalation and exhalation. Respiration signals from each run were first smoothed and then scaled to have a mean of 0 and standard deviation of 1. The cued sniff waveforms were extracted from each trial, and inhalation peak flow, duration, and volume were computed. In the pre-drug session, there were no systematic differences in peak flow ($F_{3.4,105.52} = 1.44$, $P = 0.23$, repeated measures ANOVA) or duration ($F_{3.97,123.18} = 0.89$, $P = 0.47$) across odors, but the inhalation volumes were different ($F_{3.93,121.88} = 3.27$, $P = 0.014$). Therefore the inhalation volume was included in the fMRI analysis as a nuisance regressor (see below).

fMRI data acquisition

Gradient-echo T2*-weighted echoplanar images were acquired with a Siemens Trio 3T scanner using parallel imaging and a 12-channel head-coil (repetition time, 2.3s; echo time, 20ms; matrix size, 128 × 120 voxels; field-of-view, 220 × 206mm; in-plane resolution, 1.72 × 1.72mm; slice thickness, 2mm; gap, 1mm). A 1 mm^3 T1-weighted MRI scan was also obtained for defining anatomical regions of interest (ROIs).

fMRI pre-processing

fMRI data were pre-processed with SPM8 software (http://www.fil.ion.ucl.ac.uk/spm/). All functional images across pre- and post-drug sessions were spatially realigned to the first scan of the first run to correct for head movement. The T1 structural image was also co-registered to the mean aligned functional image. Realigned functional images were then normalized into a standard space using the transformation parameter from each individual's T1-weighted scan to the standard T1 template. For multivariate fMRI analysis of olfactory and visual categorization scans, we did not perform subsequent spatial smoothing in order to preserve the voxel-wise fidelity of the signal. Images from visual localizer scans were smoothed for generating functional visual object recognition ROIs.

fMRI data analysis

General linear model

For each subject, a general linear model (GLM) was specified for each categorization scanning run in pre- or post-drug sessions from the spatially aligned, normalized, and unsmoothed fMRI data. An event-related GLM was created by modeling sniff or image onset times of each

condition independently with stick (delta) functions, and then convolving with a canonical hemodynamic response function (HRF to generate 6 regressors of interest. This model also included one regressor of no interest (catch trial onsets), six movement parameters derived from spatial realignment, and one sniff parameter (for olfactory scans) derived from inhalation volume convolved with HRF and orthogonalized with the main odor events. The data were high-pass filtered (cutoff period of 128s) to remove signal drifts, and temporal autocorrelation was adjusted using an AR(1) process. Voxel-wise, odor/image-specific β values were then estimated.

To localize visual object recognition ROIs, a block-design GLM was built on normalized and smoothed localizer scans by modeling each image block onset with a boxcar predictor convolved with HRF. Voxel-wise, condition-specific β values were estimated for object and scramble conditions. Subsequently, the contrast of object > scramble from each subject was entered into a one-sample t-test model at the group level to look for voxels that responded more strongly to objects than scrambles. Continuous clusters of voxels in bilateral LOC ($p<0.00001$, peak coordinate: right LOC, x = 44, y = -76, z = -6; left LOC, -44, -80, -2; MNI coordinate space) and fusiform cortex ($p<0.001$, right: 38, -34, -22; left: -40, -52, -20) were selected as visual ROIs.

Multivariate pattern analysis

Following GLM estimation, we extracted 36 β pattern vectors (one vector for each of the 6 odors/images and each of the 6 runs) from all voxels within anatomically defined bilateral ROIs, manually drawn on the mean image of normalized T1 scans of all subjects, using MRIcron software (http://www.mccauslandcenter.sc.edu/mricro/mricron/). A human brain atlas was used to help delineate the anatomical borders of anterior and posterior piriform cortex (APC and

PPC), amygdala, and hippocampus (Mai et al 1997). The boundary of anterior and posterior hippocampus was delineated at the uncal apex (y = -21 in MNI space) (Poppenk et al 2013). The delineation of olfactory OFC was guided by an olfactory fMRI meta-analysis (Gottfried & Zald 2005). The entorhinal cortex was drawn with reference to an MR volumetric analysis of the human entorhinal cortex (Insausti et al 1998). Visual ROIs of LOC and fusiform were defined by the independent functional localizer scan, as described above.

For multivariate pattern analysis, because we focused on information encoded in distributed fMRI patterns, the pattern vectors from the left and right hemisphere of each ROI were individually scaled to have a mean of 0 and standard deviation of 1, and then concatenated together for bilateral ROI pattern analysis. This assures that the mean signal and any lateralization of activity does not account for information coding.

The LIBSVM (Library for Support Vector Machines, https://www.csie.ntu.edu.tw/~cjlin/libsvm/) implementation was used to decode category information from patterns within a given ROI at baseline (Chang & Lin 2011). We trained the SVM classifier to separate pairs of odors of different categories (e.g. C1 vs. M1) using all six runs, and then tested the SVM by classifying odor patterns of corresponding categories but different identities (C2 vs. M2). Because the training set and testing set contain odors of different identities, significant above-chance decoding is only possible when the patterns code category-specific information independent of the identities.

Based on the regions identified by the SVM classifier in the baseline (pre-drug) session, pattern

correlation analysis was then applied to these data, in an effort to characterize changes in pattern completion and separation from pre- to post-drug sessions. Pattern dissimilarity (correlation distance) between presented stimuli was estimated by computing the linear correlation coefficient between vectors of β patterns across pairs of runs and subtracting from 1 (thus, maximal similarity = minimal distance = 0). Across-category and within-category odor distances were calculated by subtracting within-odor correlation distances (e.g., C1 in run 1 vs. C1 in run 2) from across-odor correlation distances (e.g., C1 in run 1 vs. M1 in run2), with all possible pair-wise comparisons tested. A category coding index was then computed by subtracting within-category distance from across-category distance (perfect categorization = 2, with maximal across-category distance and minimal within-category distance).

Statistics

Results are shown as mean ± s.e.m. for subjects and sessions. For determining category encoding regions, we used one-tailed *t* tests to compare decoding accuracy to chance. To test for drug effects on behavior and fMRI patterns, we used a mixed-model 2-way ANOVA, with one between-group "drug" factor (placebo/baclofen) and one repeated-measures within-subject factors of "session" (pre/post). Here the critical contrast was the group × session interaction, with post-hoc *t* tests where appropriate. Significance threshold was set at $p<0.05$, two-tailed, unless otherwise stated. Pearson's linear correlation coefficient was calculated for the correlation analysis of behavioral and fMRI pattern data across subjects.

2.4 Results

The experiment spanned 5 days (**Fig. 2.1a**). On day 1, subjects underwent pre-drug cognitive and

psychophysical testing and fMRI scanning (**Fig. 2.1c**). They were subsequently administered either placebo (n = 18) or increasing doses of baclofen (n = 14) for 5 consecutive days, in a double-blind design. This 5-day schedule was adopted to reach a target dose of 50-mg baclofen while minimizing the occurrence of side effects (Terrier et al 2011). After taking the final dose on day 5, subjects underwent the same testing and fMRI scanning procedures as in the pre-drug session. During scanning, subjects completed an olfactory categorization task, as well as a control visual categorization task to establish the sensory specificity of the imaging findings.

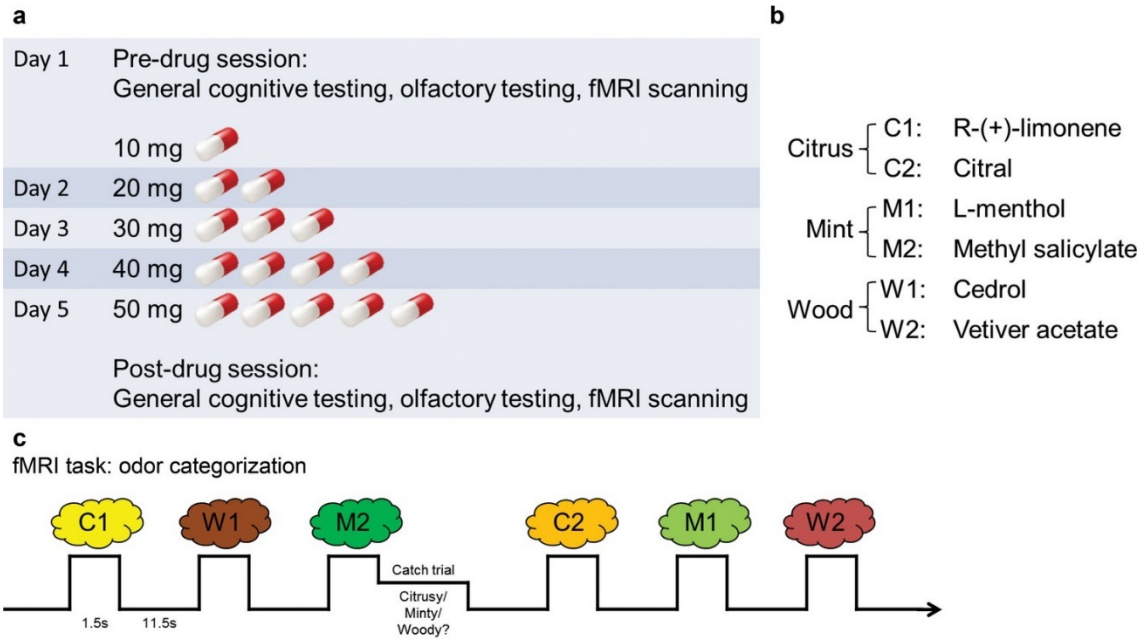

Figure 2.1 Experimental design.
a, Timeline of the 5-d experiment involving pre- and post-drug test sessions and the drug administration schedule. **b**, The six odorants included two stimuli for each of the three categories (citrus, mint, and wood). **c**, Paradigm of the fMRI odor categorization experiment. Subjects were prompted to sniff when an odorant was presented. They were asked to focus on the quality of the odor. In 14% of the trials (designated as catch trials), after the odor presentation, a screen with the names of the three categories appeared and subjects indicated the category of the received odor with a mouse click.

General cognition and olfactory perception

We first established that baclofen did not generally compromise cognitive or perceptual

performance. Specifically, we found no significant differences between baclofen and placebo groups on neuropsychological assessments of basic cognition, short-term memory, visual attention, or task switching (**Table 2.1**). We also collected subjective reports of sleepiness using the Stanford Sleepiness Scale (SSS) during test sessions, given that the most common adverse reaction to baclofen medication is transient drowsiness (RxList The internet Drug Index 2007.). Baclofen subjects reported feeling sleepier after taking the drug (**Fig. 2.2**), though reaction times during the fMRI categorization task did not differ from placebo subjects (**Table 2.1**). Finally, we examined whether baclofen altered general odor perception. Placebo and baclofen groups did not differ on olfactory measures of detection threshold, identification, discrimination, or intensity and pleasantness ratings (for stimuli used in the main fMRI experiment) (**Table 2.1**), thereby reducing the possibility that baclofen-induced changes in odor perception could have influenced the imaging results.

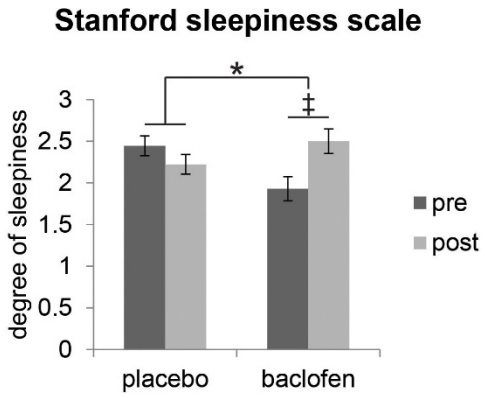

Figure 2.2 Effect of baclofen on subjective sleepiness.
Ratings from the Stanford Sleepiness Scale (1 = "wide awake", 7 = "sleep onset soon", mean ± within-subject s.e.m., placebo n = 18, baclofen n = 14) indicate that there was a significant interaction between drug groups (placebo vs. baclofen) and session (pre vs. post) ($F_{1,30} = 4.57$, $P = 0.041$; *$P < 0.05$). Post-hoc within-group comparisons showed no effect of session in placebo subjects ($F_{1,17} = 0.88$, $P = 0.36$), and a marginal effect of session in baclofen subjects ($F_{1,13} = 3.85$, ‡$P = 0.072$).

Table 2.1 Behavioral performance

Task	Placebo (n = 18)		Baclofen (n = 14)		P value of group × session interaction
	Pre	Post	Pre	Post	
MMSE	29.89±0.11	29.94±0.06	29.93±0.07	30.00±0	0.86
Digit span (forward)	7.22±0.22	7.72±0.14	7.14±0.31	7.43±0.20	0.55
Digit span (backward)	6.00±0.20	6.00±0.29	5.57±0.31	5.71±0.27	0.69
Trail making test B (s)	48.32±2.70	39.05±2.01	57.62±5.42	47.11±5.67	0.85
Stanford sleepiness scale	2.44±0.17	2.22±0.21	1.93±0.20	2.50±0.33	0.041*
Sniffin' Sticks (odor detection threshold)	7.08±0.84	9.65±1.06	7.82±0.95	8.57±1.01	0.22
UPSIT (odor identification)	36.28±0.61	36.00±0.56	34.57±0.49	33.79±0.63	0.55
α- vs. β-pinene triangle test (fine odor discrimination)	0.66±0.05	0.72±0.05	0.72±0.05	0.73±0.07	0.45
Odor intensity ratings	4.00±0.32	4.13±0.31	3.05±0.18	2.91±0.28	0.39
Odor pleasantness ratings	5.43±0.16	5.63±0.16	5.64±0.13	5.63±0.16	0.12
Odor category descriptor ratings (within – across)	7.47±0.44	7.49±0.36	7.44±0.46	7.78±0.34	0.59
Odor pairwise similarity ratings (within – across)	4.16±0.60	5.14±0.55	3.93±0.32	4.53±0.44	0.59
Odor categorization catch trial accuracy	0.87±0.04	0.89±0.03	0.81±0.04	0.81±0.04	0.80
Odor categorization catch trial RT (s)	3.29±0.23	2.85±0.15	3.89±0.38	3.48±0.34	0.93
Visual categorization catch trial accuracy	0.97±0.01 (n = 14)	0.99±0.004	0.97±0.01 (n = 11)	0.96±0.01	0.21
Visual categorization catch trial RT (s)	0.42±0.02	0.40±0.03	0.44±0.04	0.52±0.06	0.25

Data are shown for cognitive and olfactory tests, as well as for behavioral performance in fMRI experiments from placebo and baclofen groups in pre- and post-drug sessions. Scores are presented as mean ± s.e.m. P values reported are for the interaction effects between group and session, based on a 2-way ANOVA, with one between-group "drug" factor (placebo/baclofen) and one within-subject "session"

factor (pre/post). *, $P < 0.05$.

Odor perceptual categorization

Before and after drug administration, subjects participated in an fMRI odor categorization task. On each trial, subjects smelled one of six odors belonging to three categories: citrus (C1 and C2), mint (M1 and M2), and wood (W1 and W2) (**Fig. 2.1b**). Prior to each scanning session, subjects first provided category descriptor ratings (i.e., "how citrusy/minty/woody is odor X?"), as well as pair-wise similarity ratings, for each of the six odors. Both descriptor and similarity ratings from the pre-drug session showed that subjects were able to categorize the odors successfully (**Fig. 2.3**). To quantify these category effects, we calculated the difference between within-category and across-category descriptor ratings. In the pre-drug session, placebo and baclofen subjects performed equally well ($t_{30} = 0.04$, $P = 0.97$). Similarly, in the pre-drug session, for pair-wise similarity ratings, the difference of within-category and across-category similarities did not differ between groups ($t_{30} = 0.31$, $P = 0.76$). Finally, session-related changes in descriptor ratings and similarity ratings from pre- to post-drug did not differ between baclofen and placebo groups (**Table 2.1**), indicating that baclofen did not affect behavioral measures of odor categorization at the group level.

During fMRI scanning, subjects received occasional "catch trials" (every 4-8 trials), in which they were prompted to indicate the category of the previously delivered odor. In the pre-drug session, subjects categorized odors with high accuracy (84.4% ± 2.7%, chance level at 33%, $t_{31} = 19.37$, $P < 0.0001$). Of note, neither the catch trial accuracies nor reaction times (RT) differed significantly as a function of treatment group from pre- to post-drug session (**Table 2.1**).

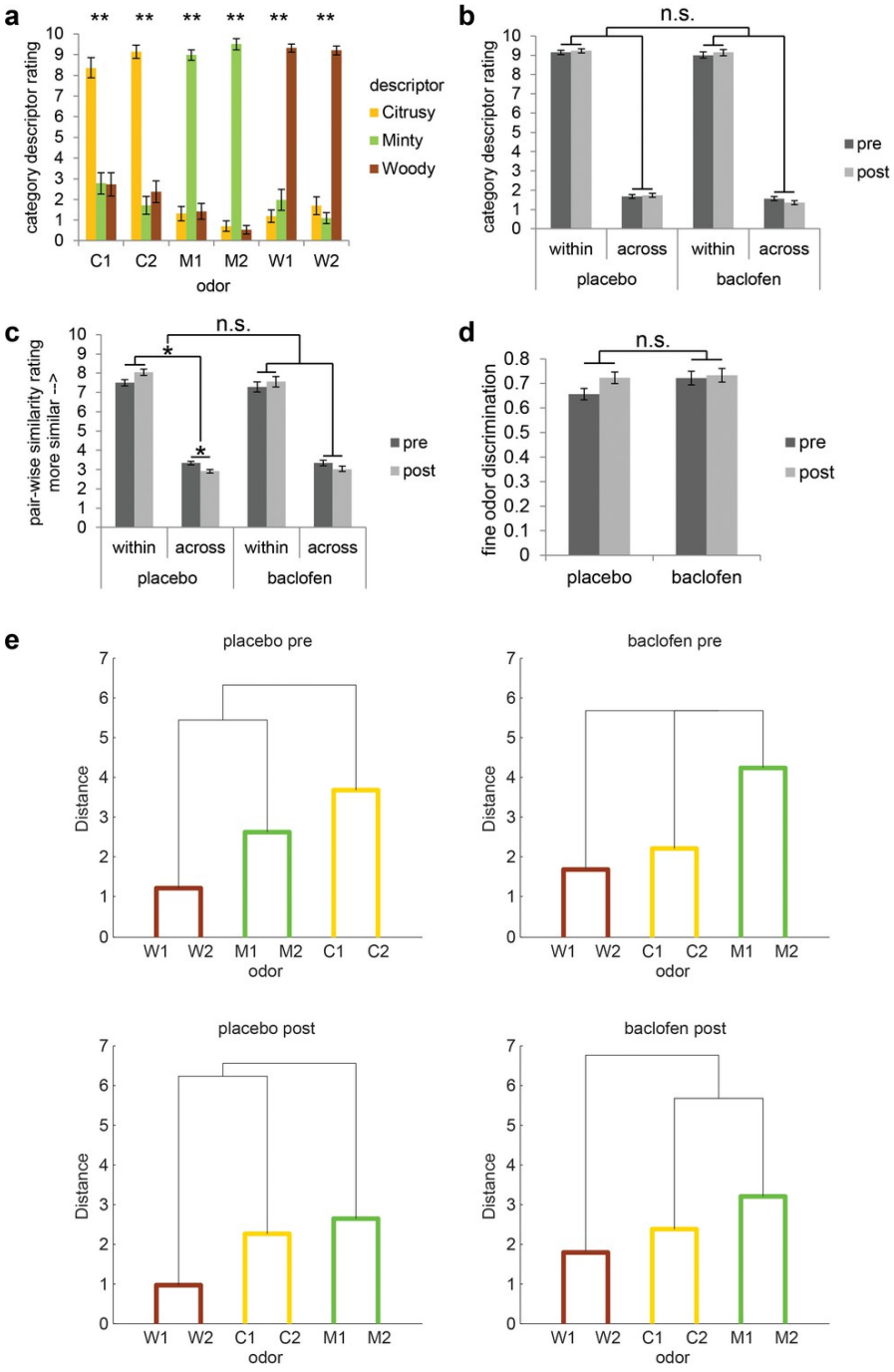

Figure 2.3 Subjects successfully classified odors into their relevant categories.
a, Category descriptor ratings of the six odors (two citrus: C1, C2; two minty: M1, M2; two woody: W1, W2) from all subjects during the pre-drug session (mean ± within-subject s.e.m., n = 32). Repeated-measures ANOVA was conducted separately on each odor (** = P < 0.001). Subjects robustly classified the odors into the appropriate perceptual categories (C1: $F_{1.86, 57.77} = 31.62$; C2: $F_{1.72, 53.40} = 74.58$; M1: $F_{1.92, 59.61} = 144.04$; M2: $F_{1.60, 49.46} = 373.79$; W1: $F_{1.82, 56.33} = 140.96$; W2: $F_{1.49, 46.10} = 166.84$; all P's < 0.001). **b,** Average of category descriptor ratings across odors, sorted by within-category condition and across-category condition in pre- and post-drug sessions for placebo (n = 18) and baclofen (n = 14, mean

± within-subject s.e.m.) groups. **c,** Pair-wise similarity ratings of within- and across-category odor pairs in pre- and post-drug sessions for placebo and baclofen groups (mean ± within-subject s.e.m.). **d,** Fine odor discrimination between α- and β-pinene in pre- and post-drug sessions for placebo and baclofen groups (mean ± within-subject s.e.m.). **e,** Dendrogram plots obtained from a cluster analysis of the average pair-wise similarity ratings for placebo and baclofen subjects during pre- and post-drug sessions showed that both groups sorted the six odors into three categories in both sessions. Shorter distance indicates greater similarity.

Category-specific ensemble codes in PPC, OFC, amygdala and pHIP

During the fMRI odor categorization task, the six odors were delivered in a pseudorandom order, and subjects were cued to sniff upon odor delivery. They were asked to pay attention to the quality of the odors throughout the task, and make category judgments during catch trials.

As olfactory information takes the form of distributed patterns of fMRI activity in the human brain (Howard et al 2009, Wu et al 2012), multivariate pattern analyses are well-suited for examining the impact of baclofen on odor pattern recognition. We first used a support vector machine (SVM) classifier to identify brain areas where odor category information is represented, among several regions of interest (ROIs) including piriform cortex, higher-order areas that directly project to piriform (olfactory subregion of OFC, amygdala, entorhinal cortex), and hippocampus (**Fig. 2.4a**). This analysis was conducted for all subjects in the pre-drug session. We trained the SVM classifier on patterns evoked by one pair of odors belonging to different categories (e.g., C1 vs. M1), and then tested the classifier on patterns evoked by the complementary pair of odors from the same categories (e.g., C2 vs. M2; **Fig. 2.4b**). Importantly, because training and test sets were based on data evoked by different odor identities, significant above-chance decoding is only possible if fMRI patterns encode category information independent of the specific odor identities. Across all subjects in the pre-drug session, we found significant above-chance decoding accuracy in PPC ($t_{31} = 2.05$, $P = 0.024$), OFC ($t_{31} = 1.96$, $P =$

0.029), amygdala (t_{31} = 3.17, P = 0.0017), and posterior hippocampus (pHIP, t_{31} = 1.90, P = 0.034; **Fig. 2.4c**). All subsequent analyses were constrained to these four regions where fMRI ensemble patterns encode odor category information.

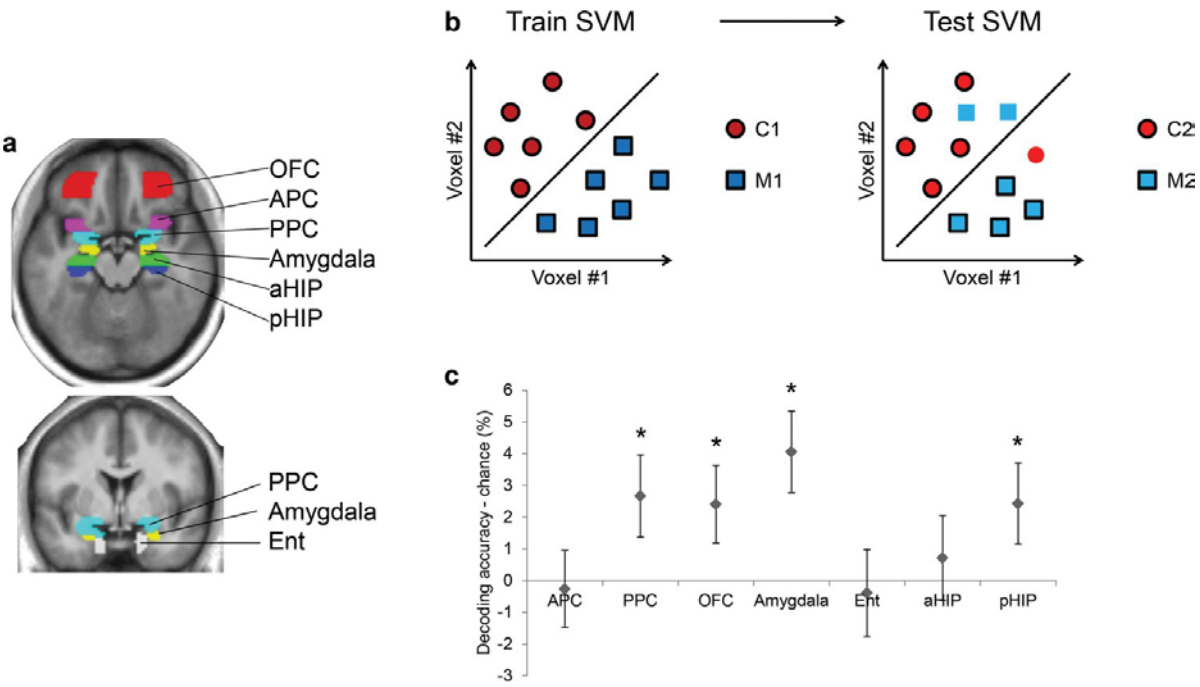

Figure 2.4 Ensemble pattern coding of odor category information at baseline (pre-baclofen session).
a, Axial and coronal slices of the averaged, normalized T1-weighted structural scan from all subjects showing anatomically defined regions of interest. Odor-evoked ensemble patterns across all voxels within a given ROI were used in a two-step multivariate classification analysis. First, we trained a linear SVM on a training data-set (**b,** left panel) to separate two odors belonging to different categories. Second, odor category coding was assessed in an independent test data-set (**b,** right panel), specifically by testing how well the SVM classified the other pair of odors from the corresponding categories; here, cross-decoding is only successful if similar patterns code different odors of the same category. **c,** Category decoding from all subjects during the pre-drug session showed that classification accuracy in PPC, OFC, amygdala, and pHIP significantly exceeded chance (mean ± between-subject s.e.m., n = 32, *P < 0.05, one-tailed).

Baclofen disrupts within-category odor discrimination in PPC

In order to characterize the continuous degree of pattern similarity between stimuli (Nili et al 2014), we next used a linear correlation analysis (Haxby et al 2001, Howard et al 2009,

Kriegeskorte et al 2008a), which provides a more direct assessment of pattern overlap. Specifically, to examine how baclofen alters the categorical organization of odors, we assembled vectors of ensemble pattern activity from all voxels within PPC, and measured the dissimilarity (correlation distances) of pattern vectors evoked by across-category odors (e.g., C1/M1) and within-category odors (e.g., C1/C2). We tested a three-way analysis of variance (ANOVA), with two within-subject factors of session (pre/post) and category type (within-/across-category), and one between-subject factor of drug (placebo/baclofen). This yielded a significant session × category type × drug interaction effect ($F_{1,30} = 5.49$, $P = 0.026$) in the absence of other main effects or two-way interactions (all P's >0.15), and suggests that baclofen significantly altered the categorical structure of odor pattern representations in PPC.

As a way to characterize the effects of baclofen on olfactory categorization in PPC, we derived a categorical coding index by subtracting within-category pattern distances from across-category pattern distances (higher value indicating better categorization, **Fig. 2.5a**). Changes from pre- to post-treatment were then compared between baclofen and placebo groups. Interestingly, in PPC the change in categorization index was significantly higher in PPC for the baclofen group, relative to the placebo group, from pre- to post-treatment (**Fig. 2.5b**), suggesting that baclofen promoted emergence of greater distinctiveness among categories. Of course, the categorization index is composed of an across-category effect and a within-category effect, meaning that the baclofen-induced enhancement of categorization could be due to greater separation of *across-category* odors (e.g., C1 and M1 patterns becoming more distinct; **Fig. 2.5a, i**) or less separation of *within-category* odors (e.g., C1 and C2 patterns becoming more similar; **Fig. 2.5a, ii**), or both. Therefore, we examined these two components separately. We found a significant session × drug

interaction effect ($F_{1,30}$ = 7.36, P = 0.011) in within-category odor distance in PPC, decreasing across sessions in the baclofen (vs. placebo) group, consistent with reduced pattern separation (**Fig. 2.5c**). In contrast, changes in across-category odor distance in PPC did not differ between the two groups (session × drug interaction: $F_{1,30}$ = 0.00014, P = 0.99; **Fig. 2.5c**). This finding suggests that associative connections in PPC are involved in preserving representational differences among odors belonging to the same category.

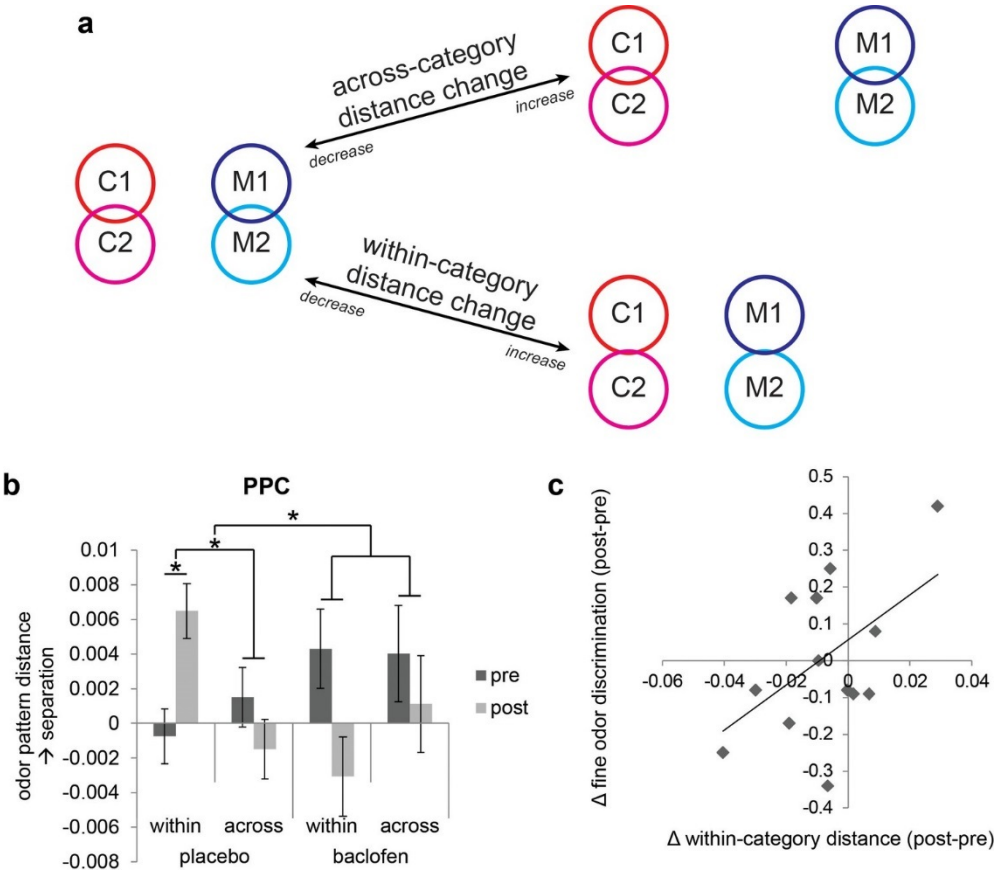

Figure 2.5 Baclofen effect on odor pattern changes in PPC.
a, Schematic illustrating within-category and across-category relationships among categorically organized odors, and how changes of each distance parameter alter the categorical structure. Worse categorization emerges when within-category distances increase or when across-category distances decrease. Better categorization emerges when within-category distances decrease or when across-category distances increase. **b,** Odor pattern distance in PPC in pre- and post-drug sessions, sorted by within-category and across-category distances, from placebo (n = 18) and baclofen (n = 14, mean ± within-subject s.e.m.) subjects. Placebo subjects showed increased within-category distances without across-category

changes. There was no significant odor distance change in baclofen subjects. **c,** A scatterplot showing the correlation between the magnitude of within-category odor pattern separation in PPC and behavioral changes in a fine odor-discrimination task, from pre- to post-drug session ($\rho = 0.51$, $P = 0.031$, $n = 14$, one-tailed). Each diamond represents one baclofen subject. *P<0.05.

If pattern separation in PPC is critical for sustaining stimulus fidelity for categorically related odors, it follows that subjects with greater disruption of PPC pattern separation (as a result of baclofen treatment) should exhibit greater olfactory perceptual deficits. This hypothesis was tested by regressing subject-wise measures of fine odor discrimination against the magnitude of baclofen-induced pattern changes in PPC. We found a significant correlation between perceptual performance and the degree of odor-evoked pattern separation in PPC ($\rho = 0.51$, $P = 0.031$, one-tailed; **Fig. 2.5d**). Thus, subjects with less within-category odor separation in PPC showed greater difficulty in discriminating between odors sharing semantic features.

Baclofen disrupts category coding in OFC and pHIP

Because olfactory categorical codes were also identified in OFC, amygdala, and pHIP in the pre-treatment session (**Fig. 2.4**), we also investigated the effects of baclofen on categorical organization of odor ensemble patterns in these regions. Significant three-way interactions of session × category type × drug were found in OFC ($F_{1,30}=4.48$, $P = 0.043$) and pHIP ($F_{1,30}=5.90$, $P = 0.021$) without other main effects or two-way interactions. No significant interaction was observed in amygdala ($F_{1,30}=0.047$, $P = 0.83$; **Fig. 2.6c**). Following the same approach used for PPC, we next asked how changes in the categorization index differ between baclofen and placebo. This interaction was driven by a significant decrease in the categorization index in OFC (**Fig. 2.6a**) and pHIP (**Fig. 2.6b**), in direct contrast to the index increase in PPC.

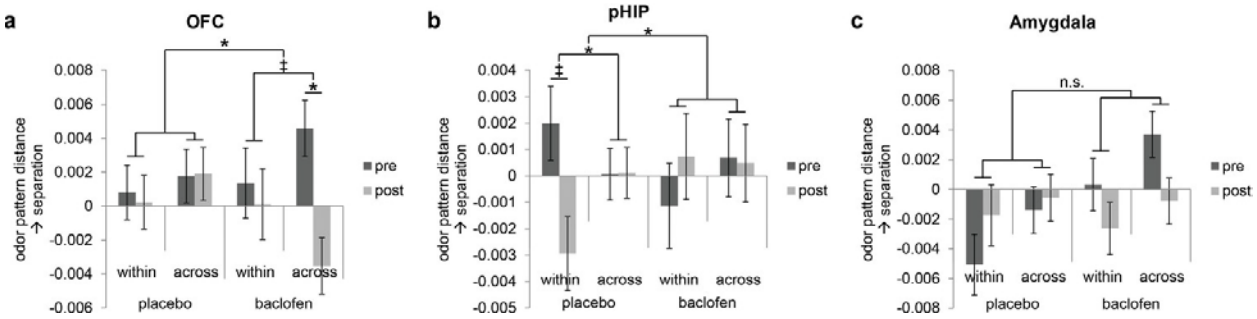

Figure 2.6 Baclofen effect on odor pattern changes in OFC and pHIP.
Odor pattern distances in OFC, pHIP, and amygdala in pre- and post-drug sessions, sorted by within-category and across-category distances, for placebo (n = 18) and baclofen (n = 14, mean ± within-subject s.e.m.) subjects. **a,** In the baclofen group, across-category distances in OFC decreased significantly without change in within-category distances, leading to disrupted categorical structure. There was no change in the placebo group. **b,** In pHIP, the placebo group showed a trend decrease in within-category odor distances without change in across-category distances. There was no significant odor distance change in the baclofen group. **c,** In amygdala there was no baclofen effect on the categorical representation of odors. ‡ P<0.1, * P<0.05.

We then considered whether disruption of category coding was due to a decrease in across-category separation or an increase in within-category separation (**Fig. 2.6d**), either of which would compromise categorical coding. In OFC, baclofen (vs. placebo) marginally reduced across-category odor separation, suggesting a reduction of categorical boundaries (**Fig. 2.6f**), with a trend effect in the session × drug interaction ($F_{1,30}$=3.21, P = 0.083), in the absence of within-category changes (session × drug interaction: $F_{1,30}$=0.02, P = 0.90). In pHIP, no significant interaction effects were found in either across-category separation ($F_{1,30}$=0.01, P = 0.94) or within-category separation ($F_{1,30}$=2.53, P = 0.12) (**Fig. 2.6f**).

Effects of baclofen are specific to olfactory processing

The above findings indicate that baclofen had selective effects on odor category coding in PPC, OFC, and pHIP. However, because baclofen was administered systemically, it remains unclear whether the effects were specific to odor categorization, or merely altered semantic or conceptual

processing independently of sensory modality. Therefore, in a parallel fMRI experiment, the same subjects performed a visual categorization task (**Fig. 2.7a**), viewing six images belonging to three categories (chairs, teapots, and houses) and identifying the category on catch trials. There was no effect of baclofen on response accuracies and reaction times (**Table 2.1**).

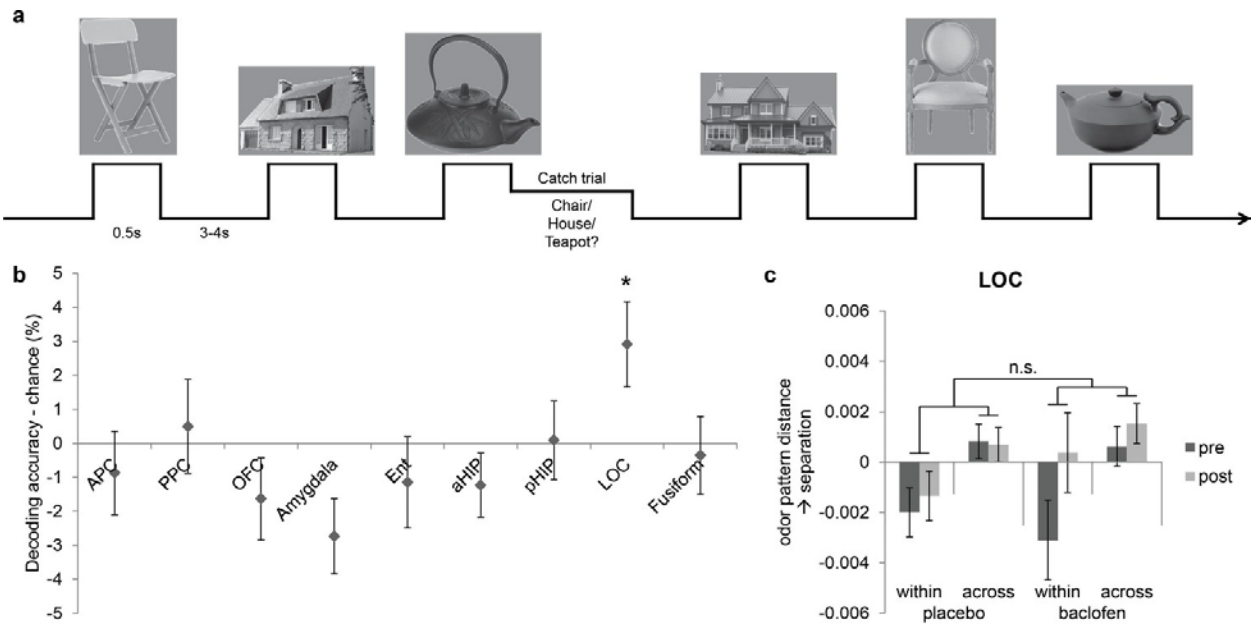

Figure 2.7 Visual control experiment.
a, Paradigm of the fMRI visual categorization experiment. Subjects viewed six images belonging to three categories. On catch trials that occasionally followed image presentations, names of the three categories appeared on screen, and subjects indicated the category of the image with a mouse click. **b,** Visual category decoding from all subjects during the pre-drug session showed that classification accuracy in LOC significantly exceeded chance (*P = 0.013, one-tailed). **c,** The effect of baclofen on visual categorical representations in LOC was not significant (P = 0.50).

We then utilized the same multivariate analysis pipeline to explore the effects of baclofen on visual pattern recognition. First we used the SVM classifier to decode visual category information in the same ROIs as in the olfactory task. We also included two additional visual ROIs located in lateral occipital complex (LOC) and fusiform gyrus as defined by an independent functional localizer scan, and which are known to be involved in visual object

recognition (Cox & Savoy 2003, Grill-Spector 2003, Haxby et al 2001, Kriegeskorte et al 2008b). Across all subjects in the pre-drug session, category decoding accuracy was significantly above chance in LOC (t_{30} = 2.33, P = 0.013), but not in fusiform cortex (t_{30} = -1.20, P = 0.88) or in any of the olfactory ROIs (PPC: t_{30} = 0.36, P = 0.72; OFC: t_{30} = -1.36, P = 0.18; amygdala: t_{30} = -2.47, P = 0.99; pHIP: t_{30} = 0.078, P = 0.47; **Fig. 2.7b**). Next, we performed an fMRI pattern correlation analysis to test the drug effect on visual category representations. A three-way session × category type × drug interaction was not significant in LOC ($F_{1,29}$=0.46, P = 0.50; **Fig. 2.7c**), suggesting that baclofen did not alter coding of categories in the visual domain.

Finally, we compared the effect of baclofen on the categorization index between olfactory and visual tasks, and found that the impact of baclofen on category coding in PPC was specific to olfaction. A mixed three-way ANOVA (two within-subject factors of modality and session; one between-subject factor of group) revealed a significant interaction of modality × session × drug ($F_{1,29}$ = 4.41, P = 0.044). Thus, while baclofen enhanced odor category coding in PPC, it did not alter the visual categorization index compared to placebo (session × drug interaction: $F_{1,29}$=0.056, P = 0.81). These findings imply that the observed effect of baclofen in PPC was not due to generic changes in semantic processing, nor to non-specific changes in hemodynamic parameters, but instead was due to alterations in information coding in the presence of olfactory inputs.

2.5 Discussion

In this study we investigated the role of piriform associative connections in the neural coding of odor categories. We used the GABA(B) receptor agonist, baclofen, to reduce associative input in

the olfactory network while sparing afferent input from the periphery. This pharmacological manipulation, combined with multivariate pattern analysis, enabled us to examine how baclofen treatment alters fMRI pattern representations of odors within and across categories relative to placebo. We found that in PPC, baclofen selectively disrupted discrimination of odors belonging to the same categorical class. The magnitude of this change correlated with difficulties in fine-odor discrimination at the perceptual level. In contrast, baclofen selectively disrupted category coding in olfactory downstream regions of OFC and pHIP.

Interestingly, the baclofen effect observed in PPC was opposite to our original prediction that baclofen would simply weaken the boundaries between categories, leading to reduced pattern separation between citrus, mint, and wood odors. Instead, reduced pattern separation among odors belonging to the *same category* was observed following baclofen administration. For example, the piriform representations of the two citrus odors became more alike, or more overlapping under baclofen. We speculate that piriform associative input normally supports the separation of patterns corresponding to unique identities of individual odors, especially those sharing perceptual features and associated with the same semantic labels. This mechanism would be compatible with prior work showing that perceptual learning enhances discriminability of within-category odor pairs, with concomitant fMRI changes in PPC as well as OFC (Li et al 2006).

It is worth considering why baclofen had no effect on across-category odor separation in PPC. One plausible explanation is that piriform cortex has the capacity to enhance either pattern separation or completion, as a function of task demands (Chapuis & Wilson 2012, Li et al 2008,

Shakhawat et al 2014). Various rodent paradigms of olfactory associative learning have shown that the direction of piriform pattern changes can flexibly match the behavioral requirements for either odor discrimination (i.e., pattern separation) or odor generalization (i.e., pattern completion). In the current experiment, subjects were asked to perform an odor categorization task, in which differences across categories, but not within category, were emphasized. As such, our experimental design might have helped stabilize category-specific differences in PPC, even in the presence of baclofen, though at the expense of within-category odor separation. The fact that categorical representations of citrus, mint, and wood odors were already highly familiar to the subjects also could have created further stability against across-category pattern changes.

In contrast to PPC, fMRI patterns in olfactory downstream areas, including OFC and pHIP, showed deficient category coding in the baclofen group. Thus in OFC, the discrete categorical patterns for citrus, mint, and wood became less separated, in the presence of baclofen. In spite of these changes, there was no parallel impact on behavior. Indeed, baclofen had no perceptual effect on categorical discrimination, and we would argue that such a finding would have been unlikely, presumably due to high familiarity and discriminability of odor categories. However, to the extent that the existence of an odor category necessitates an association between an olfactory stimulus and semantic conceptual knowledge, these results are consistent with the recognized integrative role of OFC in guiding olfactory-based behavior. Both animal and human studies have demonstrated that OFC patterns can differentiate between odor objects and categories (Critchley & Rolls 1996, Howard et al 2009, Schoenbaum & Eichenbaum 1995, Wu et al 2012). Moreover, the OFC has been proposed to integrate taste and visual information associated with odor stimuli (Critchley & Rolls 1996, Gottfried 2003), encode the reward value of odors

(Howard & Gottfried 2014), disambiguate mixtures of categorically dissimilar odors (Bowman et al 2012), and represent olfactory lexical-semantic content (Olofsson et al 2014). Viewed in this context, our results highlight the role of OFC in preserving the perceptual distinctions between different odor categories, likely through its associative access to multimodal and semantic information streams.

The demonstration of olfactory category coding in pHIP, and its vulnerability to baclofen, echoes hippocampal findings in the visual modality (Seger & Miller 2010). For example, single-unit recordings from the hippocampus have identified neurons in both humans and monkeys that are able to categorize visual information (Hampson et al 2004, Kreiman et al 2000), and fMRI activity in human hippocampus is selectively increased when memory performance relies on perceptual generalization across stimuli (Preston et al 2004, Shohamy & Wagner 2008). Considered in this framework, the effects of baclofen in pHIP may reflect a breakdown in the ability to generalize, or to make inferences, across shared odor features. It is interesting to note that both piriform cortex and hippocampus have long been regarded as canonical models of autoassociative networks where pattern separation and pattern completion computations can be flexibly achieved (Bekkers & Suzuki 2013, Eichenbaum et al 2007, Hunsaker & Kesner 2013, LaRocque et al 2013, Leutgeb & Leutgeb 2007, Wilson 2009, Yassa & Stark 2011). That the net effect of baclofen was to enhance overall categorization in PPC, but impair categorization in pHIP, highlights a unique functional difference between these two anatomically homologous regions, and may help bring new mechanistic understanding of the contributions of piriform cortex and hippocampus to human olfactory processing and perception.

Our behavioral data indicate that the 50-mg baclofen dose did not impair general cognition or olfactory perceptual performance, suggesting that off-target effects of the drug were minimal, other than a modest effect on subjective sleepiness that did not interfere with online task accuracy or response times. While it is possible that the 50-mg dose may not have been potent enough to exert a physiological effect, the study medication schedule was similar to those used in other human studies that administered baclofen to induce reliable changes in brain activity or behavior (Franklin et al 2012, Franklin et al 2011, Terrier et al 2011, Young et al 2014). One potential issue is that baclofen can also target GABA(B) receptors that have been identified in area CA1 of the hippocampus, influencing visual object recognition and memory (Ault & Nadler 1982, Lanthorn & Cotman 1981). Therefore, to establish that our findings were specific to the olfactory system, and to ensure that baclofen did not disrupt general semantic processing and object categorization, subjects also performed a visual categorization fMRI task in which they viewed pictures rather than smelled odors. This control study confirmed that our pharmacological manipulation induced both regional and modality specificity, thus ruling out possible confounds such as altered global attention, arousal, or hemodynamic reactivity. As an added way to minimize mere drug effects, we explicitly focused our imaging analyses on the interactions between group (baclofen/placebo), session (pre/post), and category level (within/across), effectively cancelling out any other session-related confounds.

An unavoidable limitation of this study was that baclofen was administered systemically. While our findings demonstrate regionally selective treatment effects in PPC, it is not possible to confirm that these changes were due to the direct action of baclofen solely at piriform cortex. There are at least three mechanisms by which baclofen could affect categorization in the

olfactory network, none of which are mutually exclusive. First, baclofen might directly target the layer 1b synapses in piriform cortex where associative intracortical and extracortical inputs predominate. This would most closely mirror what has been tested using focal baclofen injections in animal models (Barnes & Wilson 2014, Poo & Isaacson 2011), and would underscore the idea that categorical odor representations rely on associative information processing within this layer of piriform cortex. Second, baclofen might target neurons in OFC, entorhinal cortex, and other associative brain areas that project onto piriform cortex. Given that the fMRI BOLD response is thought to reflect local dendritic processing and population activity (Hipp & Siegel 2015, Logothetis & Wandell 2004), our findings could reflect a distant action of baclofen on OFC (or other areas), which in turn alters distributed fMRI patterns measured in piriform cortex. Third, the changes seen in PPC could theoretically have arisen in the olfactory bulb, where GABA(B) receptors have also been described (Aroniadou-Anderjaska et al 2000, Isaacson & Vitten 2003, Karpuk & Hayar 2008, Nickell et al 1994, Okutani et al 2003, Palouzier-Paulignan et al 2002, Wachowiak et al 2005). In this instance, one might have predicted a more profound olfactory perceptual deficit, including impairments of odor threshold, identification, and perceived intensity, though such a profile was not found in our study. Irrespective of the specific mechanism or mechanisms, these findings establish a critical role of the GABA(B) receptor in modulating categorical representations in PPC and OFC, with specificity for the olfactory modality.

In summary, our study provides a foundation for understanding the contribution of afferent and associative inputs to odor categorical perception in the human brain. Of note, this work forms a counterpoint to an earlier study from our lab in which subjects underwent a 7-day period of odor

deprivation (Wu et al 2012): by reducing olfactory afferent input, we were able to show that multivariate pattern representations of odor category were selectively altered in OFC, without any pattern-based changes observed in PPC. By comparison, in the current study, we were able to test the inverse manipulation, using baclofen to reduce olfactory associative input. In this instance, we again observed a disruption of odor categorization in OFC, but also a paradoxical enhancement of category coding in PPC, arising from reduced pattern separation of within-category odors. The fact that category pattern changes in PPC were complementary to those in OFC, as well as in pHIP, underscores the idea that odor categorization is a dynamic process involving multiple stages of an extended olfactory network. We surmise that under normal conditions, the ability to maintain discriminability of within-category odors in PPC helps prevent perceptual generalization from becoming maladaptive. With the interruption of associative input, in the setting of experimental baclofen or even perhaps as the consequence of a neurological disorder, within-category boundaries can become obscured, leading to perceptual over-generalization that can result in detrimental choices. As such, our findings may point toward an important mechanism by which associative networks regulate perceptual processing. Whether such mechanisms are restricted to the olfactory modality, or apply more widely across different sensory systems, remains to be determined.

Chapter 3: Grid-like neural representations support olfactory navigation of a two-dimensional Euclidean space

3.1 Abstract

Traditional models of spatial navigation are rooted in visual landscapes adorned with visual objects. By compiling a matrix of visual features into physical maps on a sheet of paper, or internal maps on a sheet of neurons, a navigator can accurately plan and predict a journey through space (Epstein et al 2017). However, this visuocentric perspective obscures the potential contributions of other sensory modalities to the navigation of physical spaces. In particular, many animals rely on their sense of smell to optimize approach and avoidance behaviors (Li & Liberles 2015), and the functional properties of the olfactory system, as well as the natural statistics of odor sources, are ideally suited for navigation-based responses (Catania 2013). Here we created a stimulus landscape confined to olfactory stimuli, as an initial model of how animals might encounter smells in a natural environment, and show that human subjects can mentally navigate through a two-dimensional Euclidean space composed purely of odors. During olfactory navigation, fMRI BOLD responses in entorhinal cortex (ERC) and ventromedial prefrontal cortex (vmPFC) take the form of grid-like representations with hexagonal periodicity, mimicking neural profiles in rodents during spatial navigation (Hafting et al 2005). Importantly, grid strength in ERC scaled with behavioral performance across subjects. Taken together, these findings identify grid-like codes with six-fold symmetry in the human brain as a potential mechanism for assembling odor information into spatially navigable maps, and imply more broadly that such an organization is independent of the sensory modality used to explore relational space (Aronov et al 2017, Killian et al 2012).

3.2 Introduction

A key function of sensory systems is to optimize one's physical proximity to distant objects. Sensory cues are essential for guiding animals closer to appetitive sources and further from aversive sources. Through exploration and experience, animals can adaptively learn to harness the sensory properties of their environments, enabling them not only to locate salient positions in space, but also to plan and predict the most efficient route to those positions. Across different sensory modalities, the olfactory system is uniquely suited for achieving these goals.

The sense of smell is fundamentally a predictive sense. Each sniff represents an olfactory snapshot at a specific time and place, and simultaneously represents a prediction of what odor is likely to be encountered on the next sniff, at the next time and place (Jacobs 2012). The sense of smell is also a distance sense, as airborne odors can defy physical boundaries and the absence of light in ways that visual information cannot, providing a means of identifying and tracking remote sources (Gire et al 2016). Finally, there is a relative physical constancy of an odor source, given that a lingering imprint of the odor is typically rooted at a fixed position in the environment. These features endow the olfactory system with a keen capacity for using chemical cues to navigate physical spaces. Curiously, studies examining the behavioral and neural underpinnings of odor navigation are sparse (Jacobs 2012). In the animal kingdom, olfactory cues play an indispensable role in navigation, such as foraging in insects (Reinhard et al 2004), homing behaviors in pigeons (Papi 1991), and scent-tracking in dogs (Thesen et al 1993). When blindfolded, humans are able to track odors (Porter et al 2007) and identify the direction of an odor source from distance (Welge-Lussen et al 2014). However, it is unknown whether humans can navigate a sensory space informed only by odor cues, and how the brain might internalize a

representation of two-dimensional olfactory space.

Here, we posit a world populated exclusively with odor stimuli to determine if and how a navigator – with only the luxury of the sense of smell – can traverse an olfactory landscape. Our first step was to design an ecologically plausible landscape of smells that might be naturally encountered in the environment. We took advantage of the fact that odor concentration decreases with distance from its source, and that perceived odor intensity monotonically scales with concentration (Conover 2007, Gire et al 2016, Jacobs 2012, Vickers et al 2001). To this end, we created a 2-dimensional Euclidean plane where *x*,*y* coordinates were defined by two different odors (banana and pine) that independently varied in perceived intensity from 0% to 100%, at 20% increments, forming a 6×6 space (**Fig. 3.1a, b**). Based on theoretical (Wallraff 2000) and empirical (Jacobs et al 2015) data, each position in this 2-dimensional space can be derived from the intensity of the two odors, enabling a navigator to extrapolate new information from learned odors and to predict future odor percepts, and by extension, to predict future locations (Jacobs 2012).

An important feature of our stimulus set was guided by hypotheses about how the brain would encode a mental map of odor space. In rodents, open-field foraging elicits spatially modulated activity in medial entorhinal cortex (ERC), with individual neurons (grid cells) firing at multiple discrete and hexagonally periodic locations in space (Hafting et al 2005, Stensola et al 2012). In tiling spatial fields, grid cells provide a neural metric and internalized representation for self-location, route planning, and path integration (Bush et al 2015). Similarly, humans can navigate virtual (Doeller et al 2010), visual (Julian et al 2018, Nau et al 2018), abstract (Constantinescu et

al 2016), and imagined space (Bellmund et al 2016, Horner et al 2016), inferred solely from visual inputs, with single-cell recordings (Jacobs et al 2013) and fMRI (Doeller et al 2010) techniques supporting evidence for grid-like representations in ERC as well as medial prefrontal, posterior parietal, and lateral temporal cortices (Constantinescu et al 2016, Doeller et al 2010, Jacobs et al 2013). Therefore, based on our hypothesis that navigation of an odor-informed space would rely on a grid-like coding scheme, we ensured the odor array was optimized to assess grid-like fMRI responses, including sufficient angle resolution to identify hexagonal (six-fold) symmetry, and sufficient range to characterize odor trajectories rather than odor identities per se (**Fig. 3.1c, Fig. 3.2**).

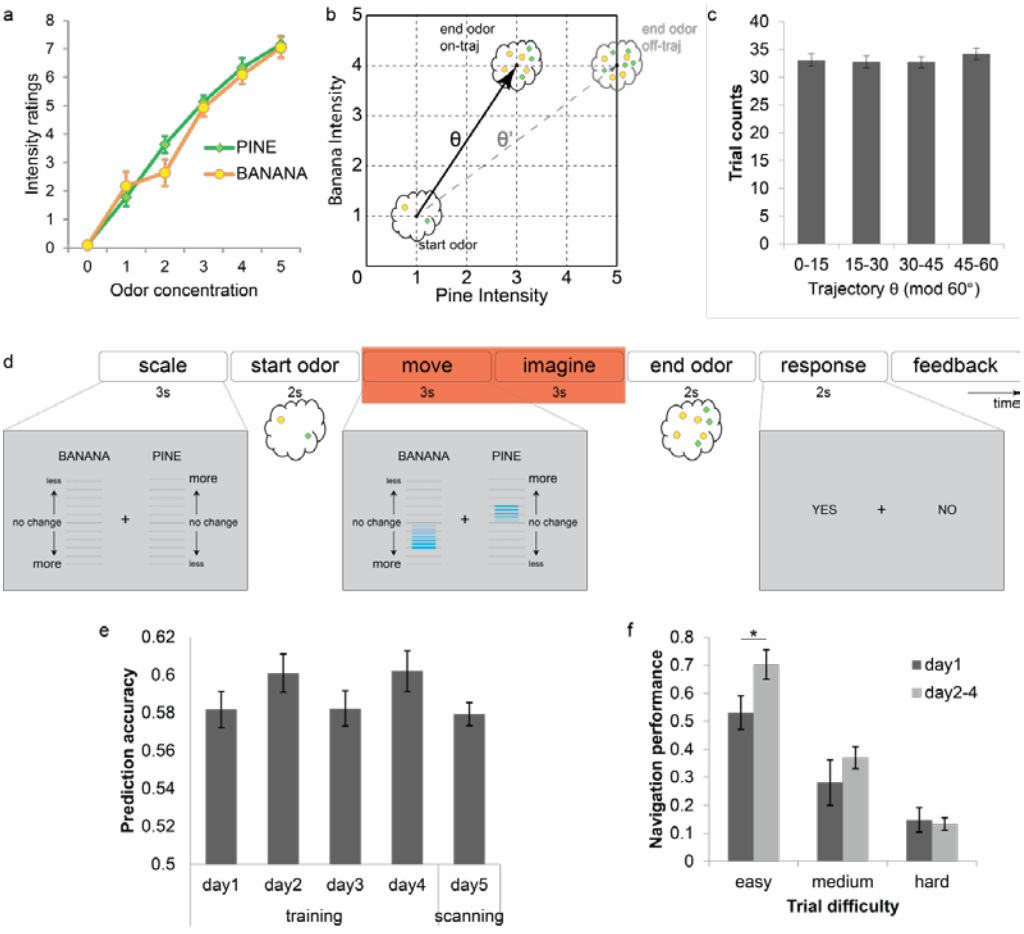

Figure 3.1 Experimental design and navigation performance.

a, Intensity ratings of pure pine and pure banana odors at different concentrations. As odor concentrations increased stepwise, subjects' perceived intensity increased stepwise as well ($F_{2.34,56.15}$=123.58, p<0.001; repeated-measures ANOVA), but ratings did not differ between the two odors at each intensity step ($F_{1,24}$=1.07, p=0.31). **b,** Conceptual layout of the odor map, in which each coordinate on the odor map corresponds to a unique mixture of the two odors. Trajectory angles were defined by start and end odor positions, and the end odor might appear on ("on-traj") or off ("off-traj") the predicted trajectory. There were three difficulty levels according to the difference between on-trajectory θ and off-trajectory θ'. Hard trials: |θ-θ'| 15°±5°; medium trials: 30°±5°; easy trials: 60°±5°. **c,** Trajectory θ was sampled evenly across the 60° cycle, with no difference in sampling frequency across directions ($F_{2.28,54.84}$=1.00, p=0.38; repeated-measures ANOVA). **d,** Timeline of an example trial of the odor prediction task. Red box indicates the time period used for the grid-cell analyses; relative movements of the banana and pine scale bars (compare left and center screenshots in grey) informed subjects how much to expect the intensities of the two odor components to change, who then indicated whether the end odor matched their prediction (right screenshot). **e,** Performance accuracy during 4 training days and the following scanning day were consistently and significantly greater than chance (50%, t_{24}>8.12, p<0.001). **f,** Navigation performance (computed as the prediction d' adjusted for perceptual discrimination on a subject-wise basis) revealed a significant effect of training, particularly for easy trials (day 1 vs. days 2-4; easy trials: t_{24}=-2.17, *p=0.04; medium trials: t_{24}=-1.01, p=0.32; hard trials: t_{24}=0.28, p=0.78; paired t-tests, two-tailed). In this and all figures, statistical tests are one-tailed unless otherwise noted; error bars, ±1 s.e.m.

To encourage mental navigation through odor space, we adapted a task similar to those used in virtual and abstract navigation studies (Constantinescu et al 2016, Doeller et al 2010). Subjects were provided a start location and a trajectory, and then assessed whether their predicted (imagined) endpoint along the trajectory corresponded to the veridical endpoint. Our task was introduced to subjects as an "odor prediction" task, but the latent structure of the map were not revealed until after the experiment. Trajectories were defined using a "start" odor mixture, along with a visual instruction screen indicating how much the intensities of banana and pine in the mixture would change upon delivery of the "end" odor (**Fig. 3.1b, d, Fig. 3.3**). After a 6-s period of mental navigation along the specified trajectory, subjects received the end odor, and indicated whether it matched their prediction. On 50% of trials the end odor was on-trajectory, and on 50% of trials the end odor was off-trajectory, varying by 15-60°. Correct answers would be compatible with successful navigation.

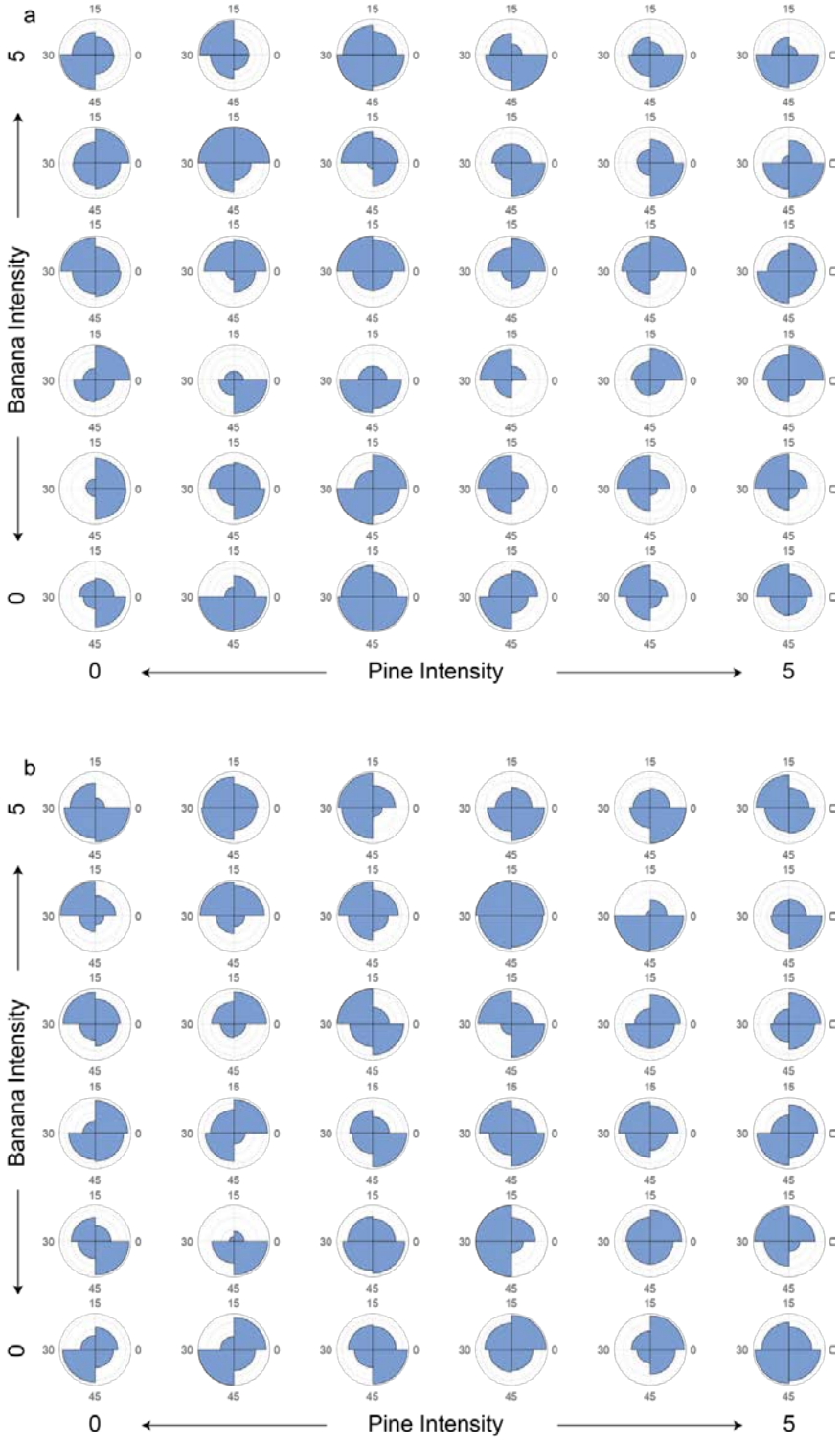

Figure 3.2 Odor trajectory θ distributions across mixtures.
a, Start odor trial trajectories (pooled from all subjects on the day of fMRI scanning), binned by 15° (modulo 60°), show that the same start odor can be associated with a wide range of different θ trajectories, and the same θ trajectory can be accessed from different start odors. These data suggest

that odor trajectory is not systematically associated with the identity of specific start odor. **b**, Likewise, the same end odor can be associated with many different θ trajectories, and the same trajectory can terminate on different end odors, implying no systematic link between trajectory and the identity of the end odor.

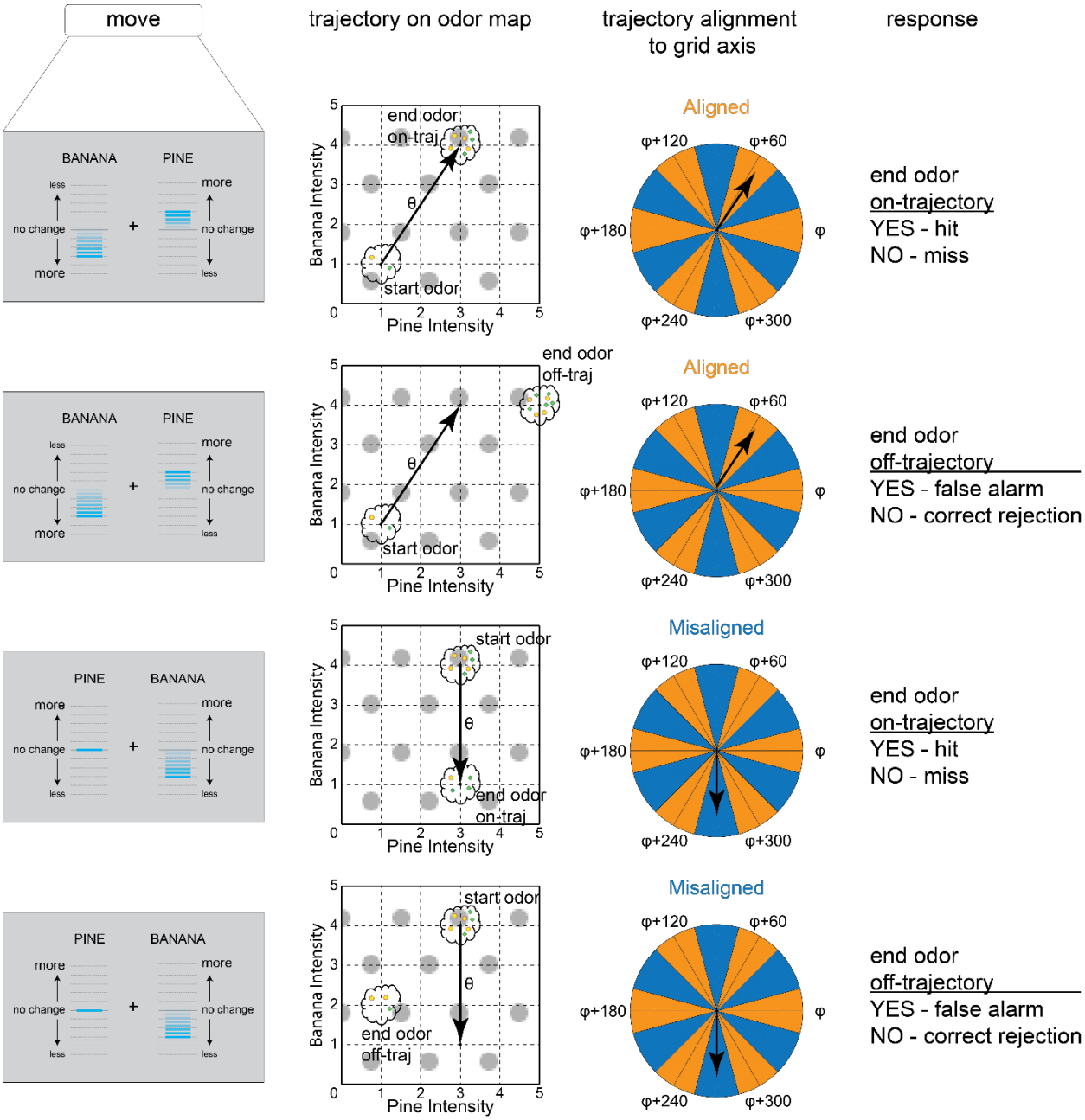

Figure 3.3 Illustration of different trial types.
The experimental design yielded 4 unique behavioral outcomes, depending on trajectory alignment and response type. First row, trial in which movement direction θ is aligned with hypothetical grid axis angle φ and the end odor lies on the trajectory; a "hit" is recorded if the end odor elicits a "yes" response, and a

"miss" is recorded if the end odor elicits a "no" response. (Small grey circles on the 6×6 grid represent a putative grid cell field with six-fold symmetry.) Second row, same as the first row, except the end odor lies off the trajectory, yielding either a "yes" response (false alarm) or "no" response (correct rejection). Third and fourth rows are similar to the upper two rows, except that these are trials in which movement direction θ is misaligned to hypothetical grid axis angle φ.

3.3 Methods

Participants and experimental design

Twenty-five participants (22 women, aged 18-37, mean age 24.3 years) completed this study. They reported to be right-handed nonsmokers with no history of significant medical illness, psychiatric disorder, or olfactory dysfunction. Fifty-two participants (40 women, age range: 18-39) gave informed consent as approved by the Northwestern University Institutional Review Board. All subjects participated in an initial screening session on day 0, which comprised an odor intensity rating task and an odor discrimination task. Thirty-four subjects who reached 70% accuracy on the odor discrimination task entered four consecutive days of behavioral training with an odor prediction task on days 1-4. Twenty-five of them who reached 60% on at least one training day then took part in an fMRI scan with the same prediction task on day 5.

Odor stimuli and delivery

Two monomolecular odorants, β-pinene (pine smell) and isoamyl acetate (banana smell) were diluted in mineral oil and matched for intensity. Odors were delivered using a custom-built air-dilution olfactometer. In the odor intensity rating task, subjects rated each pure odorant at 6 different levels of air-diluted concentrations (0%, 14.5%, 19.5%, 27%, 36.5%, and 50%). In the odor discrimination and odor prediction tasks, the two odorants, at each of the 6 concentrations, were combined into 36 different pine-banana mixtures. Each mixture represented a location in a 6×6 2-D odor space. Clean (odorless) or odorized air was directed towards subjects via Teflon

tubing at a rate of 4L/min. Subjects were cued to sniff for the odors upon viewing instructions on a computer screen.

Odor intensity rating and odor discrimination task

On the screening day, subjects first rated 6 concentrations (3 trials per concentration) of pure pine odorant and pure banana odorant on a linear visual analogue scale (anchors “not detectable” and “extremely strong”, from 0-10). Next, they performed an odor discrimination task with the pine-banana mixtures. In the discrimination task, subjects were cued to smell two odor mixtures consecutively, and were prompted to respond whether the second odor has “more pine (or banana)” or “less pine (or banana)”, compared to the first odor. During half of the trials (72 in total) they were asked to focus on discriminating pine, and the other half of trials on discriminating banana. They did not know which component they would be asked about until the choice options appeared on the screen after the second odor. The stimulus set was drawn from the “hard” trials used in the odor prediction task (see below), to ensure that subjects can perceptually discriminate between on-trajectory and off-trajectory odors spaced only 15° away from each other.

Odor prediction task

On training days 1-4 and the scanning day 5, subjects performed an odor prediction task. This task was designed to be analogous to those in virtual spatial navigation (Constantinescu et al 2016, Doeller et al 2010). The basic idea was that subjects would first smell an initial “start” odor, then mentally navigate to an “end” odor based on instructive visual cues, and finally smell a second odor, reporting whether it corresponded to their mental prediction. Subjects were

familiarized on the task with a set of 16 practice trials prior to training day 1.

At the start of a trial, subjects viewed a screen display showing two vertically oriented scale bars, one labelled “PINE” and the other labelled “BANANA” (**Fig. 3.1d**, timeline 0-3 sec). Verbal labels were placed alongside the scales: “no change” at the midpoint, and “more” and “less” at the endpoints of the scales. The labels “more” and “less” referred to the amounts of intensity change to be expected from the first sniff (first odor) to the second sniff (second odor). After viewing the scale, subjects were cued to smell an initial “start” odor (timeline 3-5 s) and instructed to pay attention to the intensities of pine and banana components in the mixture. The next part of the task was designed to encourage mental navigation in the odor space, whereby instructive cues in the visual scale bars specified the movement trajectories for a given trial. First, two bars appeared at the midpoints of each scale (“no change”), and subjects watched these bars move up and/or down along the two scales for 3 seconds (timeline 5-8 s), indicating proportional changes of the two odor components (in relation to the initial start odor). The further that each bar moved away from the midpoint, the more the respective odor component would be expected to change. In an imagination phase of the task, the same screen remained for another 3 seconds (timeline 8-11 s) as subjects actively imagined what the end odor would smell like, based on the start odor and the movements of the bars. Finally, subjects were cued to smell a second (end) odor (timeline 11-13 s), and pressed a button indicating whether they thought the end odor was on-trajectory (“YES”) or off-trajectory (“NO”). Half of the end odors were on-trajectory and half were off-trajectory. Among off-trajectory odors, there were three difficulty levels: easy, medium, and hard. The direction of the off-trajectory was 60°±5° away from the on-trajectory in easy trials, 30°±5° in medium trials, and 15°±5° in hard trials. Subjects received

feedback after their response. Another 8 s passed before the next trial began. There were 72 trials per training day, and 4-6 fMRI runs (24 trials per run) on the scanning day.

Note, across trials, the “more” and “less” labels randomly switched between top and bottom positions, and the “PINE” and “BANANA” labels randomly alternated between left and right sides of the visual display. With this randomization, imagined movement within the 2-dimensional odor space could be dissociated from mere visual cues and directional translations of the scale bars and labels.

Odor navigation index

The performance accuracy of the prediction task depended on two factors: subjects’ perceptual ability to discriminate the odor mixtures, and their memory ability to navigate to the designated location on the odor map. The former sets the upper limit of their prediction accuracy, and the latter is what we would like to capture. Therefore, we adjusted the prediction performance by the discrimination performance to derive an odor navigation measure. We calculated the sensitivity index d’ of discrimination and prediction tasks to account for response bias (Macmillan & Creelman 1990). The odor navigation index was computed as prediction d’ divided by discrimination d’.

Respiratory recording and analysis

During scanning, breathing activity was monitored using an MRI-compatible respiration transducer for MRI (BIOPAC Systems) affixed around subjects’ torso and recorded using PowerLab (ADInstruments). Breathing traces from each run were smoothed with a low-pass FIR

filter (cutoff frequency at 2 Hz) and scaled to have a mean of 0 and standard deviation of 1 (Howard et al 2016). The cued sniff waveforms were extracted from each trial. Inhalation duration and volume were computed and used as nuisance regressors in statistical modelling of the fMRI data (see below).

fMRI acquisition

Gradient-echo T2*-weighted echo-planar images (EPI) were acquired on a Siemens 3T Prisma scanner with the following parameters: repetition time (TR) = 2000 ms, echo time (TE) = 22 ms, flip angle = 80°, matrix size = 104 x 98 voxels, field of view (FoV) = 208 mm, voxel size = 2 x 2 x 2 mm^3, 58 slices per volume. The slice angle was set 15° relative to the anterior-posterior commissure line to minimize signal dropout in the basal frontal areas of the brain (Deichmann et al 2003, Weiskopf et al 2006). In addition, a field map with dual echo-time images was acquired for geometric distortion correction of the EPI functional scans, with the following parameters: TR = 555 ms, TE1 = 4.92 ms, TE2 = 7.38 ms, flip angle = 50°, FoV = 208 mm, voxel size = 2 x 2 x 2 mm^3. A 0.8 x 0.8 x 0.8 mm^3 T1-weighted structural MRI scan was also obtained to facilitate normalization of EPIs into standard space and to define piriform cortex and entorhinal cortex ROI.

Image pre-processing

fMRI data were pre-processed with SPM12 software (http://www.fil.ion.ucl.ac.uk/spm/) in Matlab. Functional images were spatially realigned to the first image in the time series, and were corrected for movement-related variance based on the field map and movement-by-distortion interactions using the Unwarp tool in SPM (Andersson et al 2001, Hutton et al 2002). The T1

structural image was co-registered to the mean aligned functional image, and underwent segmentation and spatial normalization to MNI space. Realigned functional images were normalized using the transformation parameters derived from the structural image normalization. Finally, the normalized functional images were smoothed with a 6mm full-width half-maximum Gaussian kernel. For multivariate pattern analysis in the entorhinal cortex, images were smoothed with a 2mm kernel.

Univariate analysis in whole brain

After pre-processing, we modelled fMRI time series using a set of general linear models (GLMs). All models included regressors for the main effects of the movement-and-imagination period (red box in **Fig. 3.1c**), parametric modulators of this period (see below), start odor and end odor periods, the response event, and nuisance regressors to account for head movement and differential sniff sizes. All main regressors were convolved with the canonical hemodynamic response function (HRF) in SPM. Nuisance regressors included the following: six movement parameters derived from spatial realignment, their squares, derivatives, and squares of derivatives (24 in total), within-volume slice variance and odd-vs-even slice differences, their derivatives and squares (to account for within-scan motion), breathing trace, trial-by-trial sniff volume and duration convolved with HRF and orthogonalized with the sniff events. Additional regressors were included when needed to model individual volumes that exhibited excessive head motion. Data were high-pass filtered at 1/128 Hz, and temporal autocorrelation was adjusted using an AR(1) process.

GLM1: functional localizer for hexagonal modulation

GLM1 was used as the first step to localize brain areas that showed the strongest hexagonal modulation. This analysis searched for brain areas where fMRI activity profiles fit a waveform of $\cos(6(\theta-\varphi))$, where θ is the movement trajectory direction on each trial, φ is the hypothetical axis angle of the grid field, and the factor 6 gives a 6-fold periodicity. According to the angle difference formula for cosine:

$$\cos(6(\theta-\varphi)) = (\cos6\theta*\cos6\varphi) + (\sin6\theta*\sin6\varphi)$$

the cosine term on the left side of the equation (a sinusoid with angle modulation) can be decomposed into two amplitude-modulated sinusoids, $\cos6\theta$ and $\sin6\theta$. Therefore, we created two parametric modulators for the regressor of the movement-and-imagination period (Doeller et al 2010): $\cos(6\theta)$ and $\sin(6\theta)$. We used an F-test to search for brain areas where the linear combination of the two parameter estimates (β_{cos} and β_{sin}) produced the largest amplitude. We transformed the F-statistic to a Z-statistic in each subject (Hughett 2007), and performed a 1-sample t-test across the group. To test an alternative 4-fold periodicity corresponding to a square grid, we included parametric modulators of both 4-fold and 6-fold in the same GLM.

Note that the main purpose of GLM1 was to serve as a functional localizer to identify brain regions for subsequent cross-validation analysis (GLM2; see next section). However, statistical analyses of hexagonally modulated vmPFC activity in **Figs. 3.6c-d** (derived from GLM1) should be interpreted with care. As discussed in Constantinescu et al., 2016, because of temporal autocorrelations that naturally occur in fMRI time-series data, within-subject variance at the first level of analysis can be underestimated. As such, analysis of variance (ANOVA) models to estimate six-fold symmetry can lead to an overestimation of the F-statistic at the first level, which in turn will lead to an inflated Z-score, biasing the group-level effect. Given that a direct

comparison of odor vs. visual trajectories (**Fig. 3.6d**), both of which shared the same autocorrelation structure, revealed significant effects, we believe that statistical overestimation was not a problem. Nevertheless, these considerations formed part of our rationale for conducting cross-validation analyses (GLM2) to obtain unbiased estimates of group-wise effects.

GLM2: iterative cross-validation analysis in vmPFC

To test whether the 6-fold symmetry was robust and reproducible in vmPFC, we performed a leave-one-run-out cross-validation analysis. Each subject completed 4-6 scanning runs. First, per subject, we performed GLM1 on all but one scanning run of the data ("training data"), and estimated grid angle φ for each voxel within the vmPFC ROI (cluster threshold, $p<0.001$). To this end, we averaged the parametric modulator estimates (betas; β) across all voxels in the ROI, then calculated φ as the angular coordinate mapped from Cartesian coordinates (β_{cos}, β_{sin}), divided by 6 (Doeller et al 2010). We then performed a new GLM2 on the left-out run of the data ("test data"). In GLM2, we aligned the trajectory direction θ to each individual subject's grid angle φ, and separated all directions into 12 bins of every 30° around the unit circle. We created 12 regressors for trials that belonged to each bin. At the group level, we extracted the 12 parameter estimates from the vmPFC ROI, and tested whether the resulting betas of aligned directions (0° mod 60°) were higher than misaligned directions (30° mod 60°). In the control analysis of 4-fold periodicity, we used the same approaches as above, but estimated φ with factor 4 and separated all conditions into 8 bins of every 45°.

GLM3: interregional consistency angle

This analysis was similar to GLM2, except that the grid angle φ was estimated from all runs

from the vmPFC ROI. Of note, there was no consistency of the preferred grid angle φ across subjects (**Fig. 3.4**). After modelling 12 trajectory directions, we extracted the parameter estimates from anatomically defined ROIs of entorhinal cortex (ERC), anterior piriform cortex (APC), and posterior piriform cortex (PPC). We used an ERC mask in MNI space available online from a study using high-resolution 7-T MRI (Maass et al 2015). APC and PPC were manually outlined with reference to a human brain atlas (Mai et al 1997) using MRIcron software (http://www.mccauslandcenter.sc.edu/mricro/mricron/). For each of the ROIs, we tested whether trials with directions aligned to vmPFC φ evoked higher activities than ones with misaligned directions.

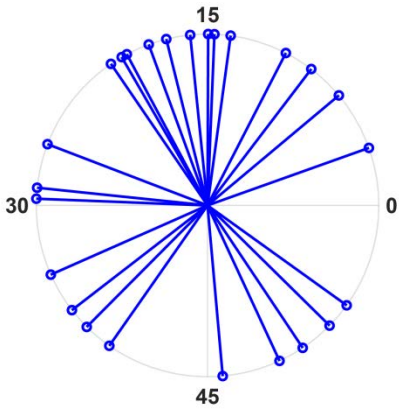

Figure 3.4 Grid axis angle φ estimated from vmPFC ROI for each subject.
Each subject has a unique estimated φ, uniformly distributed between 0-60° (Rayleigh test for non-uniformity: z=1.29, p=0.28).

Multi-voxel pattern analysis in entorhinal cortex

MVPA offers greater sensitivity to capture distributed signals in the brain compared to traditional univariate approaches (Norman et al 2006), which is particularly important in ERC, a brain region that is susceptible for distortion and signal drop-out in fMRI recordings. For this

analysis, a trial-by-trial GLM was specified for the movement-and-imagination period of each trial separately from 2mm smoothed functional images. To account fully for all variables in the task, the model also included onset times for the start odor, the end odor, and the button response. Nuisance regressors were the same as those included in the univariate analyses. Following GLM estimation, we first extracted single-trial β pattern vectors in each subject, from each and every voxel within the ERC ROI (**Fig. 3.5**). One important aspect of this analysis was to realign individual trials according to their trajectory direction θ with respect to each subject's preferred grid angle φ in vmPFC. By defining each individual's own grid angle φ, rather than relying on angle-free MVPA methods, this approach can optimize sensitivity for identifying a 6-fold periodic signal from ERC pattern correlations between trials separated by 60° increments.

In a following step, all trials (having been realigned to φ) were sorted into 12 conditions for each subject, at increments of 30° (±15°) between 0° and 330°, where 0° corresponded to φ. By way of example, for a subject with φ = 18°, all trials with θ trajectories of 18° (±15°) would be assigned to the first condition (representing φ = 0°±15°); all trials with θ trajectories of 48° (±15°) would be assigned to the second condition (representing φ = 30°±15°); and so on. Multivoxel pattern correlations (Pearson coefficients) were then computed between each and every pair of trials, and these estimates of pattern similarity were mapped onto their respective points in a 12×12 representational similarity matrix (**Fig. 3.5**). In a final step, pattern correlations derived from conditions with aligned directions (0° mod 60°) could be compared to conditions with one misaligned directions (30° mod 60°) (**Fig. 3.8b**).

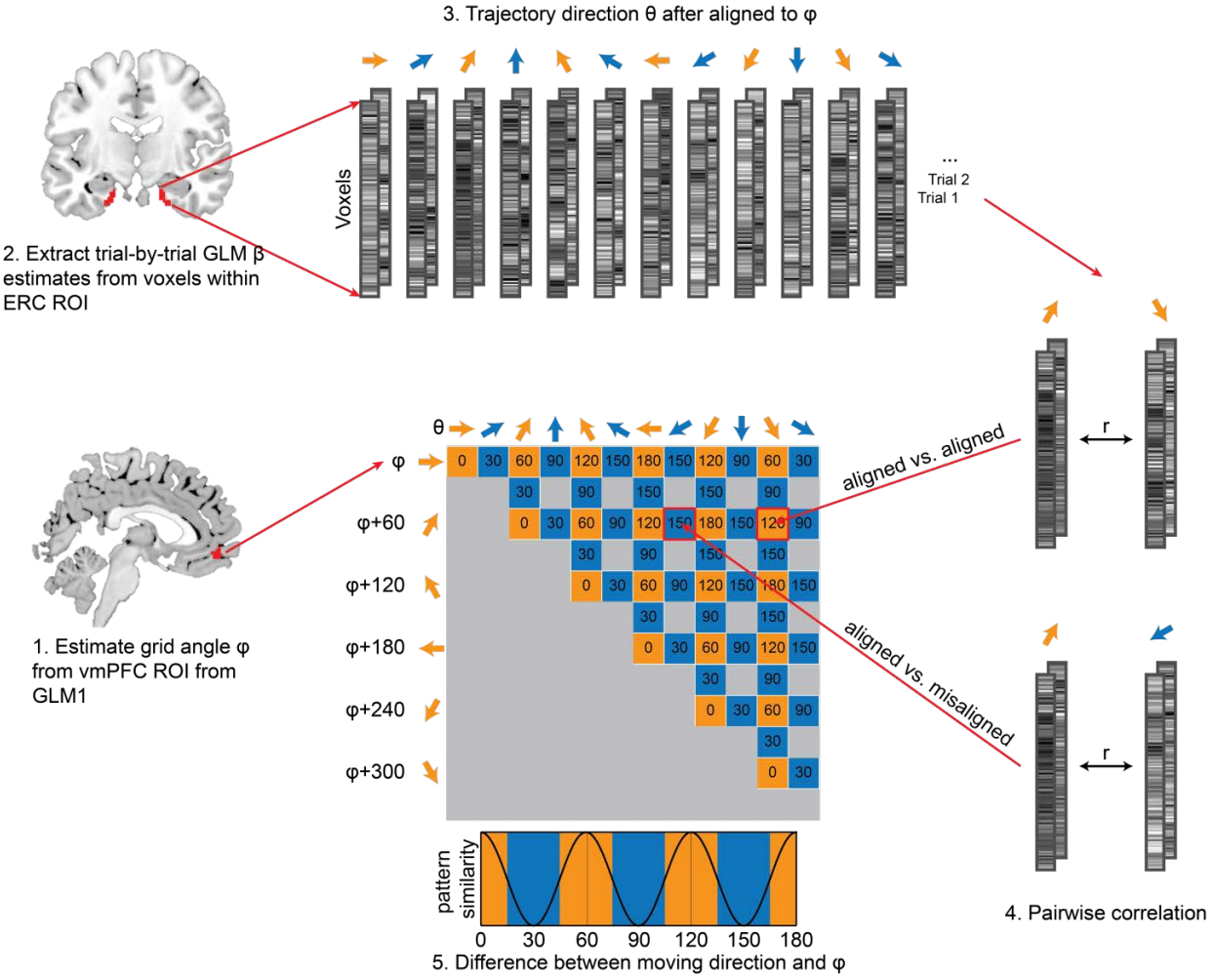

Figure 3.5 Multi-voxel pattern analysis (MVPA) method pipeline.
1. For each subject, a preferred grid axis angle φ was estimated from a vmPFC ROI defined in an initial GLM (GLM1; see main text **Fig. 3.6c**). **2.** Beta (β) estimates of a trial-by-trial GLM were extracted from voxels within an anatomically defined ROI of entorhinal cortex, and then vectorized as linear patterns. **3.** Next, the odor trajectory θ for each trial was aligned to each subject's grid angle φ, and then sorted into successive 30° bins with reference to φ. **4.** Pearson correlation coefficients were computed between each and every pair of θ trajectories, on a trial-by-trial basis, and mapped onto their respective positions in a 12×12 pattern similarity matrix (collapsed onto the upper right triangle). **5.** Finally, the correlation values were sorted according to the absolute angular difference between trials, and tested whether patterns from trial pairs aligned to the grid angle were more similar than pairs with one misaligned trial. In the similarity matrix, orange boxes represent correlations between conditions aligned to 60° increments of φ, and blue boxes represent correlations where one condition was misaligned at 30° offsets from φ. Comparisons between orange and blue boxes formed the key contrast of interest. Note, the greyed-out boxes represent correlations of no interest, as neither of these condition pairs was aligned to φ and therefore would have elicited patterns with low signal and high noise.

Statistics

Error bars throughout figures are shown as mean ± s.e.m. across subjects (n=25). In figures showing the contrast of aligned vs. misaligned conditions with 60° periodicity, bar plots were mean-corrected within subjects. The significance threshold was set at $p<0.05$ one-tailed for testing brain areas showing effects of aligned > misaligned directions, as well as testing 6-fold > 4-fold periodicity, based on our directional hypotheses (Julian et al 2018). Significance threshold was otherwise set at $p<0.05$ two-tailed.

3.4 Results

Twenty-five subjects underwent behavioral training on the prediction task for 4 days, followed by fMRI scanning on day 5. Two different measures of task performance suggested that subjects internalized mental maps of the odor space. First, prediction accuracy was consistently higher than chance (50%) on training and scan days (**Fig. 3.1e**), though no significant difference was observed across days (repeated-measures ANOVA, $F_{3.41,81.91}=1.41$, $p=0.24$). Second, we used signal detection methods to derive a navigation index, which adjusted for subject-specific olfactory perceptual limits (Methods). This analysis revealed an effect of training on navigation performance, particularly for easier trials in which the "off-trajectory" end odor was at a larger angle from the instructed trajectory, with a significant performance gain from day 1 to subsequent days ($t_{24}=-2.17$, $p=0.04$; paired t-test, two-tailed; **Fig. 3.1f**). Collectively these findings indicate that human subjects can generate predictions of to-be-encountered odors that vary in magnitude across two independent feature dimensions.

We next asked whether the human brain uses a grid-like architecture as a metric of odor space. Because most grid cells share a common grid-axis angle in the same animal (Hafting et al 2005,

Sargolini et al 2006), the group activities of grid cells can be manifested in fMRI signals showing a hexagonal periodicity as a function of moving direction (**Fig. 3.6a, b**). Such profiles have been identified in ERC and medial prefrontal cortex in neuroimaging studies of human navigation (Bellmund et al 2016, Constantinescu et al 2016, Doeller et al 2010, Horner et al 2016, Julian et al 2018, Nau et al 2018). Here, we first searched for regions where fMRI signals were hexagonally modulated by the odor trajectory direction θ during the navigation period (**Fig. 3.1d**). Using a quadrature filter (effectively, a pair of sine and cosine regressors with 60° periodicities (Doeller et al 2010); Methods), we identified the largest cluster in ventromedial prefrontal cortex (vmPFC, **Fig. 3.6c**).

Our 6-fold model of odor space included the "movement" period of the task, in which vertical translations of two visual bars informed upcoming changes in odor intensity. To minimize the possibility that the observed grid-like effects could be attributed to visual stimulation, we ensured the positions of the odor columns ("pine" and "banana") and the axis labels ("more" and "less") were randomly alternated across trials, dissociating spatial changes in visual features from magnitude changes in odor features. As a formal test that grid-like maps in vmPFC were not driven by visual confounds, we designed a complementary model in which θ was determined by the absolute directions and translations of the visual bars (**Fig. 3.7**). Visual stimulation had no significant effect on grid-like vmPFC representations, and the emergence of hexagonally modulated activity was specific for odor vs. visual trajectory (**Fig. 3.6d**).

To assess the reproducibility of these effects in vmPFC, we performed a leave-one-out cross-validation analysis to test whether the 6-fold periodic signals conform to a consistent grid-axis

angle across time. Using N-1 scan runs, we estimated each subject's grid angle φ from the vmPFC, and reserved the left-out (N^{th}) run as the test set, which was organized into 12 conditions by binning trials into successive 30° bins relative to φ. The key prediction was that fMRI activity would be higher for trials aligned to φ (0° modulo 60°) than those misaligned (30° modulo 60°). Using this unbiased analysis, we confirmed that the same grid angle was consistently identified in vmPFC (**Fig. 3.6e**), implying stability of grid angle over the duration of the experiment. This effect was specific to 6-fold symmetry: a control analysis based on a 4-fold periodicity, corresponding to a square grid field, did not elicit significant modulation in vmPFC (**Fig. 3.6f**).

Using the same approach we tested whether other brain regions might align to the same vmPFC angle (**Fig. 3.6g**). The demonstration of interregional angle stability would support the idea that a coordinated network of regions – tuned to the same grid angle – helps direct navigation of an odor space. Here we focused on ERC, based on its prominent role in grid cell coding (Doeller et al 2010, Hafting et al 2005), and anterior and posterior piriform cortex (APC, PPC), given that our task centers on exploration of olfactory space (Giessel & Datta 2014). Of note, mean fMRI signal activity in APC varied in a 6-fold symmetric manner, entrained to the same angle as in vmPFC (**Fig. 3.6h**). A similar trend was observed in PPC but was not significant (aligned>misaligned, t_{24}=2.02, p=0.027, Bonferroni adjusted α=0.016). No hexagonal effect was found in the mean ERC signal (aligned>misaligned, t_{24}=0.19, p=0.42).

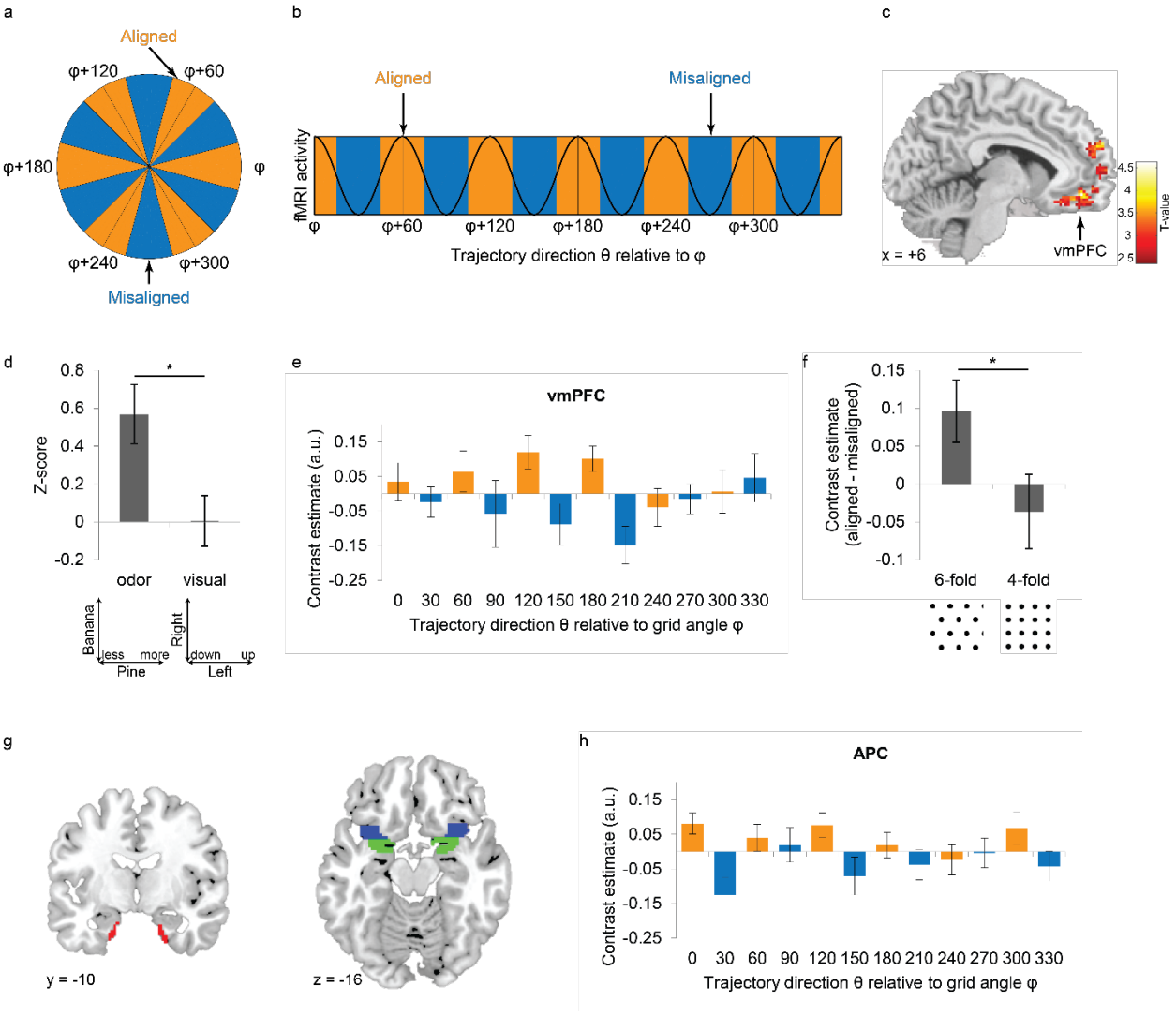

Figure 3.6 Grid-like signals during odor navigation.
a-b, Analysis schematic. Given a hexagonal grid field with main axis angle φ, trajectories on the odor map can be binned as aligned or misaligned with φ. Grid-like fMRI activity with 60° periodicity would thus be higher for aligned vs. misaligned trajectories (angle φ modulo 60° vs. angle [φ+30°] modulo 60°). **c,** Hexagonally modulated fMRI signal activity was identified in vmPFC (*x*=6, *y*=46, *z*=-10; MNI coordinate space; *Z*=3.87; cluster-level $P_{FWE\text{-}corr}$=0.0012, cluster-defining threshold p<0.001; voxel-level P_{uncorr}=0.000055). Data overlaid on a T1-weighted sagittal brain section (display threshold, p<0.01 uncorrected). **d,** Hexagonally modulated activity was not elicited in vmPFC in response to trajectories defined by the movement of the visual bars (t24=0.037, p=0.97, two-tailed); the direct comparison of odor vs. visual trajectories was significantly different (t_{24}=2.65, *p=0.0070; paired t-test). Bar plot shows condition-specific averages of voxels from a 5-mm sphere centered at the vmPFC peak in **c**. **e,** Cross-validation analysis of the grid-like effect in vmPFC (based on cluster in **c**; threshold, p<0.001) reveals grid angle reproducibility across time (aligned>misaligned; t_{24}=2.33, p=0.014). Orange/blue bars: aligned/misaligned to φ. **f,** The grid-like effect in vmPFC was specific for 6-fold, but not 4-fold periodicity (aligned>misaligned; t_{24}=-0.74, p=0.77), and the difference between 6-fold and 4-fold symmetry was significant (t_{24}=1.84, *p=0.039; paired t-test). **g,** Anatomical masks delimiting ROIs in ERC (red), APC (blue), and PPC (green). **h,** The preferred grid angle in vmPFC predicted hexagonally modulated signal in APC (aligned>misaligned; t_{24}=3.08, p=0.0026; α=0.016, Bonferroni correction for multiple comparisons of

three ROIs).

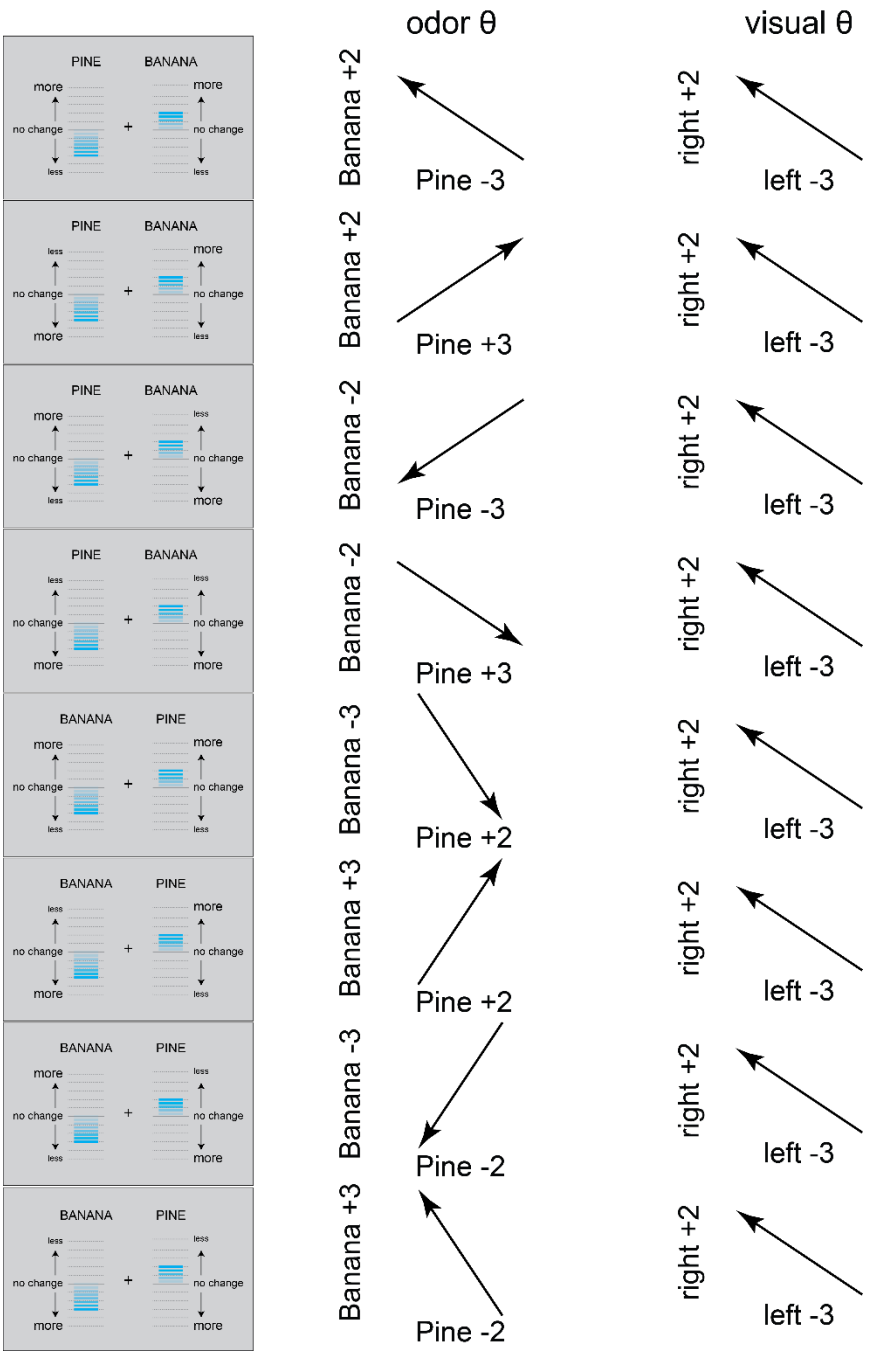

Figure 3.7 Dissociation between odor trajectory and visual trajectory.
The correspondence between visual cue and odor trajectory θ depends on the indicators on the scale. By shuffling “PINE” and “BANANA” columns, and by shuffling “more” and “less” directions, the exact same visual movement can lead to eight different odor θ trajectories. For example, in both of the top two rows, there is a -3 visual change (down-going) in the left bar and a +2 visual change (up-going) in the right bar.

However, there are unique profiles for the odor trajectories: in row one, there is a -3 pine change (less pine) and a +2 banana change (more banana), but in row two there is a +3 pine change (more pine) and a +2 banana change (more banana). Therefore, odor trajectory is uncoupled from movement changes of the visual stimuli.

Although grid-like coding in ERC was not identified in the above analysis, it is possible that ERC employs a distributed coding scheme during odor navigation (Diehl et al 2017, Hardcastle et al 2017), which might be better characterized using multi-voxel pattern-based approaches(Bellmund et al 2016). We reasoned that if distributed grid-like representations of odor space exist in ERC, then for each subject, there should be an intrinsic preferred grid angle φ (presumably aligned with vmPFC) with 60° periodicity, such that trial trajectory θ at any 60° equivalent of φ should exhibit greater pattern overlap than with 30° trajectories (**Fig. 3.8a**). A region-of-interest analysis in ERC (**Fig. 3.6g**) confirmed this prediction: after aligning trials to φ estimated from vmPFC activity, ensemble pattern similarity in ERC was significantly greater for trial pairs with trajectories aligned to the same 60° periodicity, in comparison to trial pairs in which one of the trajectories was offset by 30° (**Fig. 3.8b**). Importantly, these effects were robustly observed in the 6-fold model, but not in a 4-fold control model (**Fig. 3.8c**). Finally, to establish whether olfactory grid-like pattern representations in ERC are capable of supporting behavior, we computed the linear correlation between grid-pattern robustness (aligned vs. misaligned) and performance on the odor prediction task. Across subjects, stronger grid-like ensemble activity in ERC was associated with greater ability to predict which odor would be encountered on a specified trajectory (**Fig. 3.8d**), highlighting the involvement of this region in orienting an olfactory navigator in two-dimensional odor space.

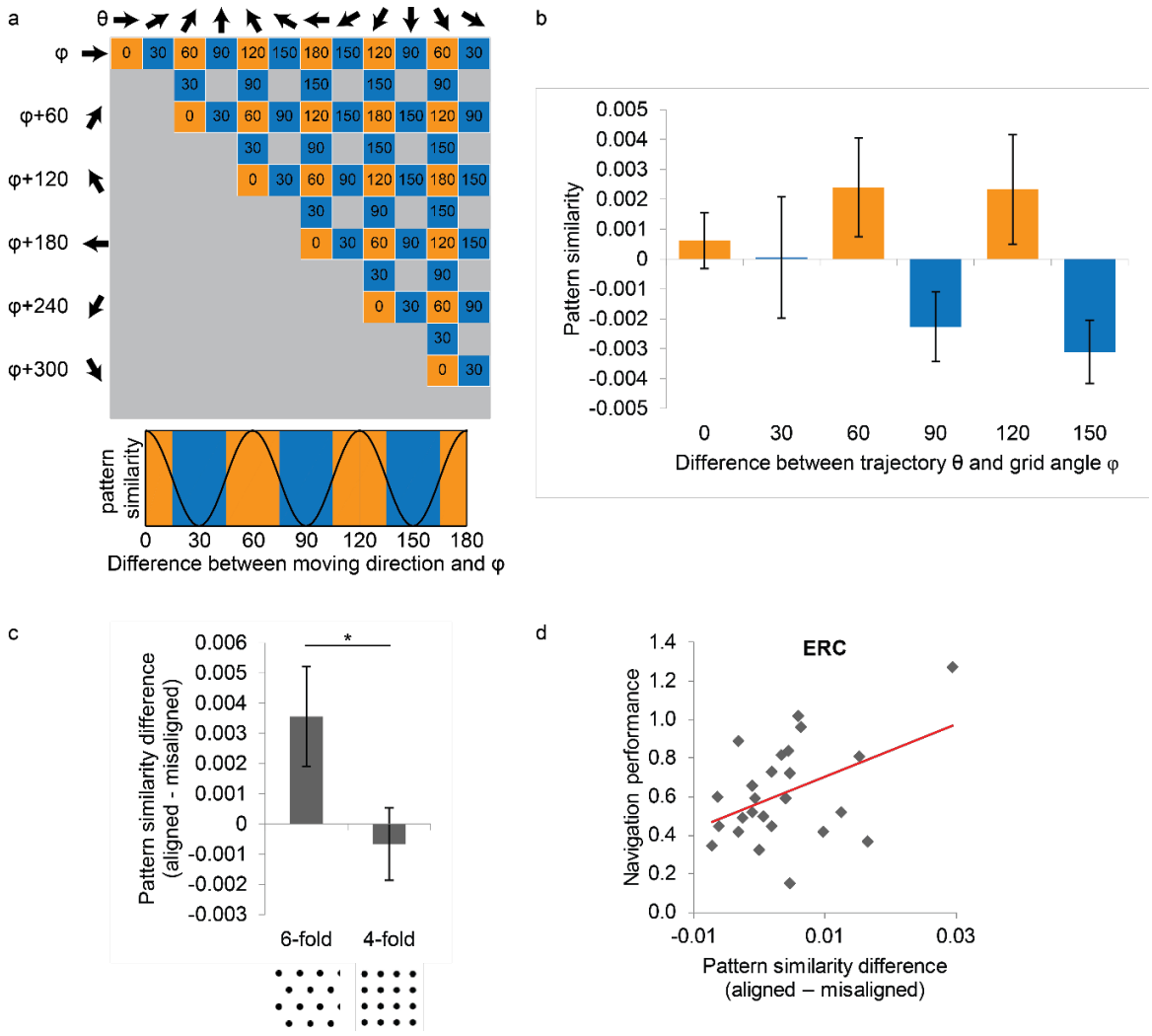

Figure 3.8 Grid-like ensemble activity in entorhinal cortex.
a, Schematic of representational similarity analysis. (Top) fMRI pattern data in ERC were organized into trajectory-specific conditions, ranging between direction θ and θ+330° (columns), where θ is aligned to each subject's preferred grid angle φ, estimated from vmPFC in **Fig. 3.6c**. Numbers at the center of each square indicate the absolute angular difference between conditions. (Bottom) Linear correlations between all trajectory pairs were then estimated, enabling a test of the hypothesis that on-trajectory patterns (directions of 0° mod 60°; orange colors) would elicit greater pattern overlap than off-trajectory patterns (directions of 30° mod 60°; blue colors). See **Fig. S3.5** for details. **b,** Pattern similarity between trajectory pairs in ERC exhibited hexagonally periodic modulation, with greater similarity for pairs aligned to grid angle φ and its 60° multiples (orange vs blue bars; aligned>misaligned, t_{24}=2.15, p=0.021). **c,** Sinusoidal modulation of ERC pattern similarity was specific to 6-fold symmetry, but not 4-fold symmetry (aligned>misaligned, t_{24}=-0.55, p=0.71), and there was a significant difference between 6-fold and 4-fold symmetry (t_{24}=2.20, *p=0.019; paired t-test). **d,** Strength of grid-like pattern representations in ERC, estimated as the difference between angle-aligned and misaligned conditions, correlated with behavioral performance (easy trials) on the odor navigation task across subjects (r=0.44, p=0.026, two-tailed).

3.5 Discussion

One striking finding is that when human subjects chart their course through odor space, fMRI-based representations in ERC, vmPFC, and APC are all aligned to the same grid angle. It is possible that different brain areas utilize hexagonal grid architectures to represent different types of mental maps, but for each of these areas to converge on the same preferred grid angle seems unlikely unless there was direct interareal coordination. A plausible alternative explanation would be that odor navigation engages hexagonally periodic activity in ERC, with feedback projections to vmPFC and APC signaling the trajectory on which the subjects is traversing through olfactory space (Carmichael & Price 1995). Information about angle alignment could be integrated with action-outcome contingencies in vmPFC to refine behavior and support more sophisticated cognitive maps (Schiller et al 2015, Wikenheiser & Schoenbaum 2016), and with olfactory information in APC to tag or strengthen a set of odor representations associated with the current trajectory.

The identification of olfactory grid-like neural representations has important implications for understanding how animals navigate through odor space. It has been suggested that odor concentration differences across sequential sniffs, and odor timing differences at each nostril, can be useful cues for tracking an olfactory source (Catania 2013, Gire et al 2016, Porter et al 2007, Rajan et al 2006). However, neither of these models is sufficient for encoding the full relational details among elements in an odorous environment. Our data highlight a novel mechanism by which the brain can construct a cognitive map of odor space. Having access to such a map would enable animals to plan how to navigate through an olfactory terrain, and to select a route that optimizes their physical proximity to odor objects. The utility of olfactory cognitive maps is

ideal for environments where odor sources are spatially and temporally anchored to a landscape, such as fruit trees, watering holes, and nesting sites, but given that grid cell fields can re-map to a new set of physical features (Diehl et al 2017, Fyhn et al 2007, Marozzi et al 2015), olfactory maps may also be effective in less stationary environments.

Chapter 4: Conclusions and future directions

Olfaction may be the most undervalued sense among the public, as typified by a 2011 McCann Worldgroup survey which found that “today's global youth would give up their sense of smell to keep their technology”. However, the olfactory system is an ideal model system to study human cognition to the eyes of a neuroscience student. It is the simplest amongst all sensory systems in terms of the number of information processing steps from receptors to high-order association areas of the brain. Its sensory pathways involve structures that are strongly implicated in emotion and memory. Odors are often perceived with hedonic judgment (Yeshurun & Sobel 2010), and often serve as a trigger of childhood memories (Willander & Larsson 2006). Olfaction provides the shortest path from the external world to its abstraction in the mind.

The two experiments described here are generally aimed at unraveling the mechanisms by which the human brain encodes odor stimuli organized with certain relationships, forming concepts of category or space. In the first experiment we sought to examine how the associative connections in the piriform cortex support neural representations of categorically organized odors. We found that application of baclofen, which specifically inhibits associative connections in both the piriform cortex and the hippocampus, elicited opposing effects in the two regions of comparable anatomy and microcircuits. Baclofen suppressed within-category discrimination in piriform cortex, but within-category generalization in hippocampus. This could reflect that intrinsic functionalities of the two regions are different in odor category coding: the piriform is responsible for maintaining discrete identities of stimuli, whereas the hippocampus assigns them to the same category through generalization. We also found that baclofen interfered with inter-

category separation in the OFC, possibly due to attenuated access to semantic information (Olofsson et al 2014).

In the first experiment, subjects were performing odor categorization (assigning category names to the stimuli) throughout the task. However, there was no name associated with the individual odor objects within the same category. One possible argument for the differential impact of baclofen on odor patterns at within-category level vs. between-category level is that, between-category odor patterns could contain and/or be stabilized by the semantic labels, the lack of which makes within-category odor patterns susceptible to change. It is unclear to what extend the semantic labels contribute to odor categorization. One alternative task could eliminate the uneven contribution of the naming processing: to include catch trials where subjects chose the name of the identity (e.g. lemon vs. orange) on some trials, and category (e.g. citrus vs. wood) on other trials. This way, the sheer effect of having semantic labels at different levels (identity vs. category) could be controlled.

The fact that baclofen was administered systemically limited our interpretation of results. We could follow up the question with a similar paradigm in animal models combining categorical odor learning, focal piriform injection of baclofen, and small animal fMRI. For example, we could train mice or rats to “categorize” odors by pairing odors with different food reward, spatial context, or sound frequencies, and examine the change of odor-evoked activity in the olfactory network as the result of local baclofen application in piriform cortex. With this hypothetical experiment, we would be able to ask whether baclofen impedes within-category odor discrimination in the piriform cortex as observed in the human study, whether it alters olfactory

bulb activity from top-down feedback changes, and how it influences odor representation in olfactory areas downstream of the piriform cortex.

The second experiment here demonstrated a grid-like representation of a two-dimensional Euclidean space inferred by mixtures of two odors varying in intensities, particularly identified in the entorhinal cortex, the vmPFC, and the piriform cortex. Our finding is in line with evidence for grid-like map structure of spaces of physical, visual, and abstract format, and supports the notion of a generalized cognitive map: the brain adopts the same fundamental mechanism to organize information systematically, in order to support a flexible strategy based on acquired knowledge in purposeful behavior.

The ability to identify directions towards behaviorally relevant sensory events within the extrapersonal space is modulated by a complex neural network responsible for memory, prediction, attention, conceptual representation, etc., in addition to the sensory representation. We speculate that grid-like maps in entorhinal cortex and vmPFC represent high-order conceptual organization of multimodal sensory events (Aronov et al 2017, Constantinescu et al 2016, Killian et al 2012). Meanwhile, it is unclear whether the grid-like map in APC is a result of top-down feedback from the entorhinal cortex, or originates endogenously from sensory inputs. This question could be approached by a uni-nostril odor navigation experiment inspired by the representational theory of olfactory attention (Mesulam 1981). Subjects would navigate the odor space with one nostril occluded. If the grid-like signal in APC originates from sensory representation of odor mixtures, we would expect such signal to be absent or attenuated from the

ipsilateral APC to the occluded nostril, whereas dissociation of APC laterality and side of occlusion would support the top-down feedback hypothesis.

We found that subjects have randomly distributed preferred grid-axis orientations without obvious clustering, as shown in studies with circular fields (Doeller et al 2010, Hafting et al 2005, Horner et al 2016). However, studies using square-shaped space found that grid axes tend to align to 7.5° from the border (Julian et al 2018, Krupic et al 2015, Stensola et al 2015). One explanation is that odor perception is inherently noisy, given that odor stimuli fluctuates with wind direction, air temperature and humidity, and intensity perception habituates with exposure. As a result, our odor space might not have a clearly perceived border, as in real and visual spaces. Indeed, it is proposed that grid-axis alignment depends on the information uncertainty of the space. Model simulations showed that self-location is decoded with maximum accuracy when the grid axes are aligned with the axis of greatest information (Schroder et al 2017). An odor space would be an excellent model to test this hypothesis, as subjects usually have differential acuities towards the odorants in the mixture, creating varying uncertainty axes in the space.

The piriform cortex emerges in both experiments, carrying information of odor category or odor space according to task demands. Although defined as the “primary” olfactory cortex due to its anatomical position, the piriform cortex functions analogous to association areas, like the fusiform cortex and the lateral occipital complex for visual category coding, and hippocampal areas for two-dimensional space mapping. In computational neuroscience, the concept of an attractor network is a popular idea to model local circuit computation as a source of pattern separation and pattern completion, as well as grid pattern emergence (McNaughton et al 2006,

Rolls 2007). In general, it is a network of neurons (nodes), often recurrently connected, whose time dynamics can settle to a stable pattern (called “attractor”). It can be traced back to Donald Hebb who proposed that co-firing neurons would be more strongly connected to each other than to the rest of the network (cells that fire together wire together), forming so-called Hebbian cell assemblies (Hebb 1949). Activity in a subset of the neurons facilitate activity in the rest of the network. The piriform cortex, which holds a rich autoassociation (recurrent) circuit, provides a sufficient anatomical substrate for attractor dynamics (Barkai & Hasselmo 1994, Patil & Hasselmo 1999). The precise capacity of the piriform cortex and its interaction with the larger network contributing to various aspects of olfactory cognition, calls for further research with thoughtful designs and technical advancement.

Understanding the neural mechanisms of how our brain can learn and remember the relationship between a myriad of information has a long way to go. The two experiments here took an olfactory approach and described two examples of associative memory with odors, seeking to contribute a drop to the ocean of the human knowledge of the brain. Advancing knowledge of olfactory coding may shed light on universal principles of sensory and memory processing. There are more interesting topics worth investigating with odors, such as learning and memory of temporal sequences of events.

References

Andersson JL, Hutton C, Ashburner J, Turner R, Friston K. 2001. Modeling geometric deformations in EPI time series. *Neuroimage* 13: 903-19

Aroniadou-Anderjaska V, Zhou FM, Priest CA, Ennis M, Shipley MT. 2000. Tonic and synaptically evoked presynaptic inhibition of sensory input to the rat olfactory bulb via GABA(B) heteroreceptors. *Journal of neurophysiology* 84: 1194-203

Aronov D, Nevers R, Tank DW. 2017. Mapping of a non-spatial dimension by the hippocampal-entorhinal circuit. *Nature* 543: 719-22

Ault B, Nadler JV. 1982. Baclofen selectively inhibits transmission at synapses made by axons of CA3 pyramidal cells in the hippocampal slice. *J Pharmacol Exp Ther* 223: 291-7

Bar M. 2007. The proactive brain: using analogies and associations to generate predictions (vol 11, pg 280, 2007). *Trends Cogn Sci* 11: 372-72

Barkai E, Hasselmo ME. 1994. Modulation of the input/output function of rat piriform cortex pyramidal cells. *Journal of neurophysiology* 72: 644-58

Barnes DC, Wilson DA. 2014. Slow-wave sleep-imposed replay modulates both strength and precision of memory. *J Neurosci* 34: 5134-42

Bekkers JM, Suzuki N. 2013. Neurons and circuits for odor processing in the piriform cortex. *Trends in neurosciences* 36: 429-38

Bellas DN, Novelly RA, Eskenazi B, Wasserstein J. 1988. The nature of unilateral neglect in the olfactory sensory system. *Neuropsychologia* 26: 45-52

Bellmund JL, Deuker L, Navarro Schroder T, Doeller CF. 2016. Grid-cell representations in mental simulation. *Elife* 5

Boccara CN, Sargolini F, Thoresen VH, Solstad T, Witter MP, et al. 2010. Grid cells in pre- and parasubiculum. *Nat Neurosci* 13: 987-94

Bowery NG. 1993. GABAB receptor pharmacology. *Annu Rev Pharmacol Toxicol* 33: 109-47

Bowery NG, Bettler B, Froestl W, Gallagher JP, Marshall F, et al. 2002. International Union of Pharmacology. XXXIII. Mammalian gamma-aminobutyric acid(B) receptors: structure and function. *Pharmacol Rev* 54: 247-64

Bowery NG, Hudson AL, Price GW. 1987. GABAA and GABAB receptor site distribution in the rat central nervous system. *Neuroscience* 20: 365-83

Bowie CR, Harvey PD. 2006. Administration and interpretation of the Trail Making Test. *Nature protocols* 1: 2277-81

Bowman NE, Kording KP, Gottfried JA. 2012. Temporal integration of olfactory perceptual evidence in human orbitofrontal cortex. *Neuron* 75: 916-27

Brennan JL, Leung JG, Gagliardi JP, Rivelli SK, Muzyk AJ. 2013. Clinical effectiveness of baclofen for the treatment of alcohol dependence: a review. *Clin Pharmacol* 5: 99-107

Bush D, Barry C, Manson D, Burgess N. 2015. Using Grid Cells for Navigation. *Neuron* 87: 507-20

Bushdid C, Magnasco MO, Vosshall LB, Keller A. 2014. Humans Can Discriminate More than 1 Trillion Olfactory Stimuli. *Science* 343: 1370-72

Carmichael ST, Clugnet MC, Price JL. 1994. Central olfactory connections in the macaque monkey. *J Comp Neurol* 346: 403-34

Carmichael ST, Price JL. 1995. Limbic Connections of the Orbital and Medial Prefrontal Cortex in Macaque Monkeys. *J. Comp. Neurol.* 363: 615-41

Castro JB, Ramanathan A, Chennubhotla CS. 2013. Categorical dimensions of human odor descriptor space revealed by non-negative matrix factorization. *PLoS One* 8: e73289

Catania KC. 2013. Stereo and serial sniffing guide navigation to an odour source in a mammal. *Nat. Commun.* 4: 1441

Cattarelli M, Astic L, Kauer JS. 1988. Metabolic Mapping of 2-Deoxyglucose Uptake in the Rat Piriform Cortex Using Computerized Image-Processing. *Brain Research* 442: 180-84

Chang C-C, Lin C-J. 2011. LIBSVM: A library for support vector machines. *ACM Trans. Intell. Syst. Technol.* 2: 1-27

Chapuis J, Wilson DA. 2012. Bidirectional plasticity of cortical pattern recognition and behavioral sensory acuity. *Nat Neurosci* 15: 155-61

Chu DC, Albin RL, Young AB, Penney JB. 1990. Distribution and kinetics of GABAB binding sites in rat central nervous system: a quantitative autoradiographic study. *Neuroscience* 34: 341-57

Conover MR. 2007. *Predator-prey dynamics : the role of olfaction*. Boca Raton: CRC Press. 248 p. pp.

Constantinescu AO, O'Reilly JX, Behrens TEJ. 2016. Organizing conceptual knowledge in humans with a gridlike code. *Science* 352: 1464-8

Courtiol E, Wilson DA. 2014. Thalamic olfaction: characterizing odor processing in the mediodorsal thalamus of the rat. *Journal of neurophysiology* 111: 1274-85

Cox DD, Savoy RL. 2003. Functional magnetic resonance imaging (fMRI) "brain reading": detecting and classifying distributed patterns of fMRI activity in human visual cortex. *NeuroImage* 19: 261-70

Critchley HD, Rolls ET. 1996. Olfactory neuronal responses in the primate orbitofrontal cortex: analysis in an olfactory discrimination task. *Journal of neurophysiology* 75: 1659-72

Deichmann R, Gottfried JA, Hutton C, Turner R. 2003. Optimized EPI for fMRI studies of the orbitofrontal cortex. *NeuroImage* 19: 430-41

Diehl GW, Hon OJ, Leutgeb S, Leutgeb JK. 2017. Grid and Nongrid Cells in Medial Entorhinal Cortex Represent Spatial Location and Environmental Features with Complementary Coding Schemes. *Neuron* 94: 83-92 e6

Doeller CF, Barry C, Burgess N. 2010. Evidence for grid cells in a human memory network. *Nature* 463: 657-61

Doty RL, Shaman P, Kimmelman CP, Dann MS. 1984. University of Pennsylvania Smell Identification Test: a rapid quantitative olfactory function test for the clinic. *The Laryngoscope* 94: 176-8

Dupouy J, Fournier JP, Jouanjus E, Palmaro A, Poutrain JC, et al. 2014. Baclofen for alcohol dependence in France: incidence of treated patients and prescription patterns--a cohort study. *Eur Neuropsychopharmacol* 24: 192-9

Eichenbaum H, Yonelinas AP, Ranganath C. 2007. The medial temporal lobe and recognition memory. *Annual review of neuroscience* 30: 123-52

Epstein RA, Patai EZ, Julian JB, Spiers HJ. 2017. The cognitive map in humans: spatial navigation and beyond. *Nat Neurosci* 20: 1504-13

Folstein MF, Folstein SE, McHugh PR. 1975. "Mini-mental state". A practical method for grading the cognitive state of patients for the clinician. *J Psychiatr Res* 12: 189-98

Franco MI, Turin L, Mershin A, Skoulakis EM. 2011. Molecular vibration-sensing component in Drosophila melanogaster olfaction. *Proceedings of the National Academy of Sciences of the United States of America* 108: 3797-802

Franklin TR, Shin J, Jagannathan K, Suh JJ, Detre JA, et al. 2012. Acute baclofen diminishes resting baseline blood flow to limbic structures: a perfusion fMRI study. *Drug and alcohol dependence* 125: 60-6

Franklin TR, Wang Z, Sciortino N, Harper D, Li Y, et al. 2011. Modulation of resting brain cerebral blood flow by the GABA B agonist, baclofen: a longitudinal perfusion fMRI study. *Drug and alcohol dependence* 117: 176-83

Franks KM, Russo MJ, Sosulski DL, Mulligan AA, Siegelbaum SA, Axel R. 2011. Recurrent Circuitry Dynamically Shapes the Activation of Piriform Cortex. *Neuron* 72: 49-56

Fyhn M, Hafting T, Treves A, Moser MB, Moser EI. 2007. Hippocampal remapping and grid realignment in entorhinal cortex. *Nature* 446: 190-4

Gagliardo A. 2013. Forty years of olfactory navigation in birds. *J Exp Biol* 216: 2165-71

Gerrard LB, Tantirigama MLS, Bekkers JM. 2018. Pre- and Postsynaptic Activation of GABA(B) Receptors Modulates Principal Cell Excitation in the Piriform Cortex. *Front Cell Neurosci* 12

Ghosh S, Larson SD, Hefzi H, Marnoy Z, Cutforth T, et al. 2011. Sensory maps in the olfactory cortex defined by long-range viral tracing of single neurons. *Nature* 472: 217-20

Giessel AJ, Datta SR. 2014. Olfactory maps, circuits and computations. *Curr. Opin. Neurobiol.* 24: 120-32

Gire DH, Kapoor V, Arrighi-Allisan A, Seminara A, Murthy VN. 2016. Mice Develop Efficient Strategies for Foraging and Navigation Using Complex Natural Stimuli. *Curr. Biol.* 26: 1261-73

Gottfried J. 2003. The Nose Smells What the Eye SeesCrossmodal Visual Facilitation of Human Olfactory Perception. *Neuron* 39: 375-86

Gottfried JA. 2010. Central mechanisms of odour object perception. *Nature reviews. Neuroscience* 11: 628-41

Gottfried JA, Winston JS, Dolan RJ. 2006. Dissociable codes of odor quality and odorant structure in human piriform cortex. *Neuron* 49: 467-79

Gottfried JA, Zald DH. 2005. On the scent of human olfactory orbitofrontal cortex: meta-analysis and comparison to non-human primates. *Brain research. Brain research reviews* 50: 287-304

Grill-Spector K. 2003. The neural basis of object perception. *Current Opinion in Neurobiology* 13: 159-66

Haberly LB. 2001. Parallel-distributed processing in olfactory cortex: new insights from morphological and physiological analysis of neuronal circuitry. *Chem Senses* 26: 551-76

Haberly LB, Bower JM. 1989. Olfactory cortex: model circuit for study of associative memory? *Trends in neurosciences* 12: 258-64

Haberly LB, Price JL. 1977. The axonal projection patterns of the mitral and tufted cells of the olfactory bulb in the rat. *Brain Res* 129: 152-7

Haberly LB, Price JL. 1978. Association and commissural fiber systems of the olfactory cortex of the rat. II. Systems originating in the olfactory peduncle. *J Comp Neurol* 181: 781-807

Hafting T, Fyhn M, Molden S, Moser MB, Moser EI. 2005. Microstructure of a spatial map in the entorhinal cortex. *Nature* 436: 801-6

Hampson RE, Pons TP, Stanford TR, Deadwyler SA. 2004. Categorization in the monkey hippocampus: a possible mechanism for encoding information into memory. *Proceedings of the National Academy of Sciences of the United States of America* 101: 3184-9

Hardcastle K, Maheswaranathan N, Ganguli S, Giocomo LM. 2017. A Multiplexed, Heterogeneous, and Adaptive Code for Navigation in Medial Entorhinal Cortex. *Neuron* 94: 375-87 e7

Hargreaves EL, Rao G, Lee I, Knierim JJ. 2005. Major dissociation between medial and lateral entorhinal input to dorsal hippocampus. *Science* 308: 1792-94

Haxby JV, Gobbini MI, Furey ML, Ishai A, Schouten JL, Pietrini P. 2001. Distributed and overlapping representations of faces and objects in ventral temporal cortex. *Science* 293: 2425-30

Hebb DO. 1949. *The organization of behavior; a neuropsychological theory*. New York,: Wiley. xix, 335 p. pp.

Hipp JF, Siegel M. 2015. BOLD fMRI Correlation Reflects Frequency-Specific Neuronal Correlation. *Current biology : CB* 25: 1368-74

Hoddes E, Zarcone V, Smythe H, Phillips R, Dement WC. 1973. Quantification of sleepiness: a new approach. *Psychophysiology* 10: 431-6

Horner AJ, Bisby JA, Zotow E, Bush D, Burgess N. 2016. Grid-like Processing of Imagined Navigation. *Curr. Biol.* 26: 842-7

Howard JD, Gottfried JA. 2014. Configural and elemental coding of natural odor mixture components in the human brain. *Neuron* 84: 857-69

Howard JD, Kahnt T, Gottfried JA. 2016. Converging prefrontal pathways support associative and perceptual features of conditioned stimuli. *Nat. Commun.* 7: 11546

Howard JD, Plailly J, Grueschow M, Haynes JD, Gottfried JA. 2009. Odor quality coding and categorization in human posterior piriform cortex. *Nat Neurosci* 12: 932-8

Hughett P. 2007. Accurate computation of the F-to-z and t-to-z transforms for large arguments. *J. Stat. Soft.* 23: 1-5

Hummel T, Sekinger B, Wolf SR, Pauli E, Kobal G. 1997. 'Sniffin' sticks': olfactory performance assessed by the combined testing of odor identification, odor discrimination and olfactory threshold. *Chem Senses* 22: 39-52

Hunsaker MR, Kesner RP. 2013. The operation of pattern separation and pattern completion processes associated with different attributes or domains of memory. *Neuroscience and biobehavioral reviews* 37: 36-58

Hutton C, Bork A, Josephs O, Deichmann R, Ashburner J, Turner R. 2002. Image distortion correction in fMRI: A quantitative evaluation. *Neuroimage* 16: 217-40

Illig KR. 2005. Projections from orbitofrontal cortex to anterior piriform cortex in the rat suggest a role in olfactory information processing. *J Comp Neurol* 488: 224-31

Illig KR, Haberly LB. 2003. Odor-evoked activity is spatially distributed in piriform cortex. *Journal of Comparative Neurology* 457: 361-73

Imai T. 2014. Construction of functional neuronal circuitry in the olfactory bulb. *Seminars in cell & developmental biology* 35: 180-8

Insausti R, Amaral DG, Cowan WM. 1987. The entorhinal cortex of the monkey: II. Cortical afferents. *J Comp Neurol* 264: 356-95

Insausti R, Juottonen K, Soininen H, Insausti AM, Partanen K, et al. 1998. MR volumetric analysis of the human entorhinal, perirhinal, and temporopolar cortices. *AJNR. American journal of neuroradiology* 19: 659-71

Insausti R, Marcos P, Arroyo-Jiménez MM, Blaizot X, Martínez-Marcos A. 2002. Comparative aspects of the olfactory portion of the entorhinal cortex and its projection to the hippocampus in rodents, nonhuman primates, and the human brain. *Brain Research Bulletin* 57: 557-60

Isaacson JS, Vitten H. 2003. GABA(B) receptors inhibit dendrodendritic transmission in the rat olfactory bulb. *J Neurosci* 23: 2032-9

Jacobs J, Weidemann CT, Miller JF, Solway A, Burke JF, et al. 2013. Direct recordings of grid-like neuronal activity in human spatial navigation. *Nat. Neurosci.* 16: 1188-90

Jacobs LF. 2012. From chemotaxis to the cognitive map: the function of olfaction. *Proc. Natl. Acad. Sci. U.S.A.* 109 Suppl 1: 10693-700

Jacobs LF, Arter J, Cook A, Sulloway FJ. 2015. Olfactory Orientation and Navigation in Humans. *PLoS One* 10: e0129387

Johnson DM, Illig KR, Behan M, Haberly LB. 2000. New features of connectivity in piriform cortex visualized by intracellular injection of pyramidal cells suggest that "primary" olfactory cortex functions like "association" cortex in other sensory systems. *J Neurosci* 20: 6974-82

Julian JB, Keinath AT, Frazzetta G, Epstein RA. 2018. Human entorhinal cortex represents visual space using a boundary-anchored grid. *Nat. Neurosci.*

Kahn R, Biswas K, Childress AR, Shoptaw S, Fudala PJ, et al. 2009. Multi-center trial of baclofen for abstinence initiation in severe cocaine-dependent individuals. *Drug and alcohol dependence* 103: 59-64

Karpuk N, Hayar A. 2008. Activation of postsynaptic GABAB receptors modulates the bursting pattern and synaptic activity of olfactory bulb juxtaglomerular neurons. *Journal of neurophysiology* 99: 308-19

Keller A, Gerkin RC, Guan Y, Dhurandhar A, Turu G, et al. 2017. Predicting human olfactory perception from chemical features of odor molecules. *Science* 355: 820-26

Killian NJ, Jutras MJ, Buffalo EA. 2012. A map of visual space in the primate entorhinal cortex. *Nature* 491: 761-4

Koulakov AA, Kolterman BE, Enikolopov AG, Rinberg D. 2011. In search of the structure of human olfactory space. *Frontiers in systems neuroscience* 5: 65

Kreiman G, Koch C, Fried I. 2000. Category-specific visual responses of single neurons in the human medial temporal lobe. *Nat Neurosci* 3: 946-53

Kriegeskorte N, Mur M, Bandettini P. 2008a. Representational similarity analysis - connecting the branches of systems neuroscience. *Frontiers in systems neuroscience* 2: 4

Kriegeskorte N, Mur M, Ruff DA, Kiani R, Bodurka J, et al. 2008b. Matching categorical object representations in inferior temporal cortex of man and monkey. *Neuron* 60: 1126-41

Krupic J, Bauza M, Burton S, Barry C, O'Keefe J. 2015. Grid cell symmetry is shaped by environmental geometry. *Nature* 518: 232-U199

Kunz L, Schroder TN, Lee H, Montag C, Lachmann B, et al. 2015. Reduced grid-cell-like representations in adults at genetic risk for Alzheimer's disease. *Science* 350: 430-33

Lanthorn TH, Cotman CW. 1981. Baclofen selectively inhibits excitatory synaptic transmission in the hippocampus. *Brain Res* 225: 171-8

LaRocque KF, Smith ME, Carr VA, Witthoft N, Grill-Spector K, Wagner AD. 2013. Global similarity and pattern separation in the human medial temporal lobe predict subsequent memory. *J Neurosci* 33: 5466-74

Leutgeb S, Leutgeb JK. 2007. Pattern separation, pattern completion, and new neuronal codes within a continuous CA3 map. *Learning & memory* 14: 745-57

Li Q, Liberles SD. 2015. Aversion and Attraction through Olfaction. *Current Biology* 25: R120-R29

Li W, Howard JD, Parrish TB, Gottfried JA. 2008. Aversive learning enhances perceptual and cortical discrimination of indiscriminable odor cues. *Science* 319: 1842-5

Li W, Luxenberg E, Parrish T, Gottfried JA. 2006. Learning to smell the roses: experience-dependent neural plasticity in human piriform and orbitofrontal cortices. *Neuron* 52: 1097-108

Logothetis NK, Wandell BA. 2004. Interpreting the BOLD signal. *Annual review of physiology* 66: 735-69

Maass A, Berron D, Libby LA, Ranganath C, Duzel E. 2015. Functional subregions of the human entorhinal cortex. *Elife* 4

Macmillan NA, Creelman CD. 1990. Response bias: Characteristics of detection theory, threshold theory, and "nonparametric" indexes. *Psychol. Bull.* 107: 401-13

Mai JK, Assheuer J, Paxinos G. 1997. *Atlas of the human brain*. San Diego, Calif.: Academic Press. viii, 328 p. pp.

Majak K, Ronkko S, Kemppainen S, Pitkanen A. 2004. Projections from the amygdaloid complex to the piriform cortex: A PHA-L study in the rat. *J Comp Neurol* 476: 414-28

Malnic B, Godfrey PA, Buck LB. 2004. The human olfactory receptor gene family. *Proceedings of the National Academy of Sciences of the United States of America* 101: 2584-9

Marozzi E, Ginzberg LL, Alenda A, Jeffery KJ. 2015. Purely Translational Realignment in Grid Cell Firing Patterns Following Nonmetric Context Change. *Cereb. Cortex.* 25: 4619-27

McGann JP, Pirez N, Gainey MA, Muratore C, Elias AS, Wachowiak M. 2005. Odorant representations are modulated by intra- but not interglomerular presynaptic inhibition of olfactory sensory neurons. *Neuron* 48: 1039-53

McNaughton BL, Battaglia FP, Jensen O, Moser EI, Moser MB. 2006. Path integration and the neural basis of the 'cognitive map'. *Nature reviews. Neuroscience* 7: 663-78

Meister M. 2015. On the dimensionality of odor space. *Elife* 4: e07865

Mesulam MM. 1981. A cortical network for directed attention and unilateral neglect. *Ann Neurol* 10: 309-25

Miyamichi K, Amat F, Moussavi F, Wang C, Wickersham I, et al. 2011. Cortical representations of olfactory input by trans-synaptic tracing. *Nature* 472: 191-6

Mori K, Nagao H, Yoshihara Y. 1999. The olfactory bulb: coding and processing of odor molecule information. *Science* 286: 711-5

Moser EI, Roudi Y, Witter MP, Kentros C, Bonhoeffer T, Moser MB. 2014. Grid cells and cortical representation. *Nature reviews. Neuroscience* 15: 466-81

Nau M, Navarro Schroder T, Bellmund JLS, Doeller CF. 2018. Hexadirectional coding of visual space in human entorhinal cortex. *Nat. Neurosci.*

Navarro Schroder T, Haak KV, Zaragoza Jimenez NI, Beckmann CF, Doeller CF. 2015. Functional topography of the human entorhinal cortex. *Elife* 4

Nickell WT, Behbehani MM, Shipley MT. 1994. Evidence for GABAB-mediated inhibition of transmission from the olfactory nerve to mitral cells in the rat olfactory bulb. *Brain Res Bull* 35: 119-23

Nili H, Wingfield C, Walther A, Su L, Marslen-Wilson W, Kriegeskorte N. 2014. A toolbox for representational similarity analysis. *PLoS computational biology* 10: e1003553

Norman KA, Polyn SM, Detre GJ, Haxby JV. 2006. Beyond mind-reading: multi-voxel pattern analysis of fMRI data. *Trends. Cogn. Sci.* 10: 424-30

O'Keefe J, Dostrovsky J. 1971. The hippocampus as a spatial map. Preliminary evidence from unit activity in the freely-moving rat. *Brain Res* 34: 171-5

Okutani F, Zhang JJ, Otsuka T, Yagi F, Kaba H. 2003. Modulation of olfactory learning in young rats through intrabulbar GABA(B) receptors. *The European journal of neuroscience* 18: 2031-6

Olofsson JK, Hurley RS, Bowman NE, Bao X, Mesulam MM, Gottfried JA. 2014. A designated odor-language integration system in the human brain. *J Neurosci* 34: 14864-73

Palouzier-Paulignan B, Duchamp-Viret P, Hardy AB, Duchamp A. 2002. GABA(B) receptor-mediated inhibition of mitral/tufted cell activity in the rat olfactory bulb: a whole-cell patch-clamp study in vitro. *Neuroscience* 111: 241-50

Papi F. 1991. Orientation in birds. Olfactory navigation. *EXS* 60: 52-85

Patil MM, Hasselmo ME. 1999. Modulation of inhibitory synaptic potentials in the piriform cortex. *Journal of neurophysiology* 81: 2103-18

Poo C, Isaacson JS. 2011. A major role for intracortical circuits in the strength and tuning of odor-evoked excitation in olfactory cortex. *Neuron* 72: 41-8

Poppenk J, Evensmoen HR, Moscovitch M, Nadel L. 2013. Long-axis specialization of the human hippocampus. *Trends Cogn Sci* 17: 230-40

Porter J, Craven B, Khan RM, Chang SJ, Kang I, et al. 2007. Mechanisms of scent-tracking in humans. *Nat. Neurosci.* 10: 27-9

Preston AR, Shrager Y, Dudukovic NM, Gabrieli JD. 2004. Hippocampal contribution to the novel use of relational information in declarative memory. *Hippocampus* 14: 148-52

Qu LP, Kahnt T, Cole SM, Gottfried JA. 2016. De Novo Emergence of Odor Category Representations in the Human Brain. *J Neurosci* 36: 468-78

Rajan R, Clement JP, Bhalla US. 2006. Rats smell in stereo. *Science* 311: 666-70

Ranganath C, Ritchey M. 2012. Two cortical systems for memory-guided behaviour. *Nature reviews. Neuroscience* 13: 713-26

Reinhard J, Srinivasan MV, Zhang S. 2004. Olfaction: scent-triggered navigation in honeybees. *Nature* 427: 411

Rennaker RL, Chen CFF, Ruyle AM, Sloan AM, Wilson DA. 2007. Spatial and temporal distribution of odorant-evoked activity in the piriform cortex. *Journal of Neuroscience* 27: 1534-42

Ressler KJ, Sullivan SL, Buck LB. 1993. A zonal organization of odorant receptor gene expression in the olfactory epithelium. *Cell* 73: 597-609

Ressler KJ, Sullivan SL, Buck LB. 1994. Information coding in the olfactory system: evidence for a stereotyped and highly organized epitope map in the olfactory bulb. *Cell* 79: 1245-55

Riesenhuber M, Poggio T. 2000. Models of object recognition. *Nat Neurosci* 3: 1199-204

Roach EH. 1978. Principles of categorization In *Cognition and Categorization*, ed. EH Rosch, BB Lloyd. Hillsdale, New Jersey: Erlbaum Associates

Rolls ET. 2007. An attractor network in the hippocampus: theory and neurophysiology. *Learning & memory* 14: 714-31

RxList The internet Drug Index. 2007. Kemstro, Side Effects and Drug Interactions.

Sargolini F, Fyhn M, Hafting T, McNaughton BL, Witter MP, et al. 2006. Conjunctive representation of position, direction, and velocity in entorhinal cortex. *Science* 312: 758-62

Schiffman SS. 1974. Physicochemical Correlates of Olfactory Quality. *Science* 185: 112-17

Schiller D, Eichenbaum H, Buffalo EA, Davachi L, Foster DJ, et al. 2015. Memory and Space: Towards an Understanding of the Cognitive Map. *J. Neurosci.* 35: 13904-11

Schoenbaum G, Eichenbaum H. 1995. Information coding in the rodent prefrontal cortex. II. Ensemble activity in orbitofrontal cortex. *Journal of neurophysiology* 74: 751-62

Schroder TN, Towse BW, Burgess N, Barry C, Doeller CF. 2017. Optimal decision making using grid cells under spatial uncertainty. *bioRxiv*

Seger CA, Miller EK. 2010. Category learning in the brain. *Annual review of neuroscience* 33: 203-19

Shakhawat AM, Harley CW, Yuan Q. 2014. Arc visualization of odor objects reveals experience-dependent ensemble sharpening, separation, and merging in anterior piriform cortex in adult rat. *J Neurosci* 34: 10206-10

Shepherd GM. 2011. The microcircuit concept applied to cortical evolution: from three-layer to six-layer cortex. *Front Neuroanat* 5: 30

Shipley MT, Ennis M. 1996. Functional organization of olfactory system. *J Neurobiol* 30: 123-76

Shohamy D, Wagner AD. 2008. Integrating memories in the human brain: hippocampal-midbrain encoding of overlapping events. *Neuron* 60: 378-89

Snitz K, Yablonka A, Weiss T, Frumin I, Khan RM, Sobel N. 2013. Predicting odor perceptual similarity from odor structure. *PLoS computational biology* 9: e1003184

Sohal VS, Hasselmo ME. 1998. GABA(B) modulation improves sequence disambiguation in computational models of hippocampal region CA3. *Hippocampus* 8: 171-93

Sosulski DL, Bloom ML, Cutforth T, Axel R, Datta SR. 2011. Distinct representations of olfactory information in different cortical centres. *Nature* 472: 213-6

Stensola H, Stensola T, Solstad T, Froland K, Moser MB, Moser EI. 2012. The entorhinal grid map is discretized. *Nature* 492: 72-78

Stensola T, Stensola H, Moser MB, Moser EI. 2015. Shearing-induced asymmetry in entorhinal grid cells. *Nature* 518: 207-12

Stettler DD, Axel R. 2009. Representations of odor in the piriform cortex. *Neuron* 63: 854-64

Stokes CCA, Isaacson JS. 2010. From Dendrite to Soma: Dynamic Routing of Inhibition by Complementary Interneuron Microcircuits in Olfactory Cortex. *Neuron* 67: 452-65

Suzuki N, Bekkers JM. 2012. Microcircuits Mediating Feedforward and Feedback Synaptic Inhibition in the Piriform Cortex. *Journal of Neuroscience* 32: 919-31

Tang AC, Hasselmo ME. 1994. Selective suppression of intrinsic but not afferent fiber synaptic transmission by baclofen in the piriform (olfactory) cortex. *Brain Res* 659: 75-81

Terrier J, Ort A, Yvon C, Saj A, Vuilleumier P, Lüscher C. 2011. Bi-Directional Effect of Increasing Doses of Baclofen on Reinforcement Learning. *Frontiers in Behavioral Neuroscience* 5

Thesen A, Steen JB, Doving KB. 1993. Behaviour of dogs during olfactory tracking. *J. Exp. Biol.* 180: 247-51

Tolman EC. 1948. Cognitive maps in rats and men. *Psychol Rev* 55: 189-208

Vassar R, Chao SK, Sitcheran R, Nunez JM, Vosshall LB, Axel R. 1994. Topographic organization of sensory projections to the olfactory bulb. *Cell* 79: 981-91

Vassar R, Ngai J, Axel R. 1993. Spatial segregation of odorant receptor expression in the mammalian olfactory epithelium. *Cell* 74: 309-18

Vaughan DN, Jackson GD. 2014. The piriform cortex and human focal epilepsy. *Front Neurol* 5

Vickers NJ, Christensen TA, Baker TC, Hildebrand JG. 2001. Odour-plume dynamics influence the brain's olfactory code. *Nature* 410: 466-70

Wachowiak M, McGann JP, Heyward PM, Shao Z, Puche AC, Shipley MT. 2005. Inhibition of olfactory receptor neuron input to olfactory bulb glomeruli mediated by suppression of presynaptic calcium influx. *Journal of neurophysiology* 94: 2700-12

Wallenstein GV, Eichenbaum H, Hasselmo ME. 1998. The hippocampus as an associator of discontiguous events. *Trends in neurosciences* 21: 317-23

Wallenstein GV, Hasselmo ME. 1997. GABAergic modulation of hippocampal population activity: sequence learning, place field development, and the phase precession effect. *Journal of neurophysiology* 78: 393-408

Wallraff HG. 2000. Simulated navigation based on observed gradients of atmospheric trace gases (Models on pigeon homing, part 3). *J. Theor. Biol.* 205: 133-45

Weiskopf N, Hutton C, Josephs O, Deichmann R. 2006. Optimal EPI parameters for reduction of susceptibility-induced BOLD sensitivity losses: a whole-brain analysis at 3 T and 1.5 T. *Neuroimage* 33: 493-504

Welge-Lussen A, Looser GL, Westermann B, Hummel T. 2014. Olfactory source localization in the open field using one or both nostrils. *Rhinology* 52: 41-7

Wenner AM, Wells PH, Johnson DL. 1969. Honey bee recruitment to food sources: olfaction or language? *Science* 164: 84-6

Wikenheiser AM, Schoenbaum G. 2016. Over the river, through the woods: cognitive maps in the hippocampus and orbitofrontal cortex. *Nat. Rev. Neurosci.* 17: 513-23

Willander J, Larsson M. 2006. Smell your way back to childhood: autobiographical odor memory. *Psychon Bull Rev* 13: 240-4

Wilson DA. 2009. Pattern separation and completion in olfaction. *Annals of the New York Academy of Sciences* 1170: 306-12

Wilson DA, Sullivan RM. 2011. Cortical processing of odor objects. *Neuron* 72: 506-19

Wu KN, Tan BK, Howard JD, Conley DB, Gottfried JA. 2012. Olfactory input is critical for sustaining odor quality codes in human orbitofrontal cortex. *Nat Neurosci* 15: 1313-9

Yassa MA, Stark CE. 2011. Pattern separation in the hippocampus. *Trends in neurosciences* 34: 515-25

Yeshurun Y, Sobel N. 2010. An odor is not worth a thousand words: from multidimensional odors to unidimensional odor objects. *Annu Rev Psychol* 61: 219-41, C1-5

Young KA, Franklin TR, Roberts DC, Jagannathan K, Suh JJ, et al. 2014. Nipping cue reactivity in the bud: baclofen prevents limbic activation elicited by subliminal drug cues. *J Neurosci* 34: 5038-43

Zhang X, Firestein S. 2002. The olfactory receptor gene superfamily of the mouse. *Nat Neurosci* 5: 124-33